Integrative small and long RNA-omics analysis of human healing and non-healing wounds discovers cooperating microRNAs as therapeutic targets

Zhuang Liu[1,6], Letian Zhang[1,6], Maria A. Toma[1], Dongqing Li[1,2], Xiaowei Bian[1], Irena Pastar[3], Marjana Tomic-Canic[3], Pehr Sommar[4]* and Ning Xu Landén[1,5]*

[1]Dermatology and Venereology Division, Department of Medicine Solna, Center for Molecular Medicine, Karolinska Institutet, 17176 Stockholm, Sweden

[2]Institute of Dermatology, Chinese Academy of Medical Sciences and Peking Union Medical College, Nanjing, Jiangsu, China

[3]Wound Healing and Regenerative Medicine Research Program, Dr Phillip Frost Department of Dermatology and Cutaneous Surgery, University of Miami Miller School of Medicine, Miami, FL, USA.

[4]Department of Plastic and Reconstructive Surgery, Karolinska University Hospital, Stockholm, Sweden

[5]Ming Wai Lau Centre for Reparative Medicine, Stockholm Node, Karolinska Institute, 17177 Stockholm, Sweden

[6]Equal contribution

*Co-senior authors

To whom correspondence should be addressed: Email: ning.xu@ki.se or pehr.sommar@regionstockholm.se

Abstract

MicroRNAs (miR) are important posttranscriptional regulators and exhibit a high potential to be utilized in diagnosis and therapy. However, our insufficient knowledge of the miR-mediated gene regulation in human skin wound healing severely hinders the identification of clinically relevant miRs. Here, we performed paired small RNA and long RNA sequencing in human tissue samples, including matched skin and acute wounds collected at each healing stage and chronic non-healing venous ulcers (VU). With integrative small and long RNA-omics analysis, we developed a compendium (https://www.xulandenlab.com/humanwounds-mirna-mrna), which will be an open, comprehensive resource to broadly aid wound healing research. With this first clinical, wound-centric resource of miRs and mRNAs, we identified 17 pathologically relevant miRs that exhibited abnormal VU expression and displayed their targets enriched explicitly in the VU gene signature. Intermeshing regulatory networks controlled by these miRs revealed their high cooperativity in contributing to chronic wound pathology characterized by persistent inflammation and proliferative phase initiation failure. Furthermore, we demonstrated that miR-34a, miR-424, and miR-516, upregulated in VU, cooperatively suppressed keratinocyte growth while promoting inflammatory response. Collectively, our study opens the possibility of developing innovative wound treatment that targets pathologically relevant cooperating miRs to attain higher therapeutic efficacy and specificity.

Keywords: microRNA, regulatory network, wound healing, chronic wound, venous ulcer

Introduction

Wound healing is a fundamental biological process comprising three sequential and overlapping phases, i.e., inflammation, proliferation, and remodeling(Reinke & Sorg, 2012). This delicate repair process is often disrupted in chronic venous insufficiency patients, resulting in venous ulcers (VU) characterized by persistent inflammation and proliferative phase initiation failure(Eming et al., 2014). VU is the most common chronic non-healing wound type, comprising 45–60% of all lower extremity ulcerations(Vivas et al., 2016). VU exhibits a marked impact on health-related life quality and represents a significant financial burden both to the patients and the society with an annual health care cost of overall $14.9 billion in the USA(Hoversten et al., 2020). A deeper understanding of the underlying gene expression regulatory mechanisms during physiological and pathological wound repair is essential for developing more effective wound treatments(Stone et al., 2017).

MicroRNAs (miR) represent a group of short (~22 nt) non-coding ribonucleic acids, incorporating into the RNA-induced silencing complex and binding to the 3' untranslated region of their target mRNAs, resulting in mRNA destabilization and translational repression(Stavast & Erkeland, 2019). Given that an individual miR can target dozens to hundreds of genes, miRs have been identified as regulators of complex gene networks(Stavast & Erkeland, 2019). MiR-mediated regulation is reportedly crucial in multiple fundamental biological processes including skin wound repair(Herter & Xu Landen, 2017; Meng et al., 2018). Importantly, manipulating miRs critical for the disease pathogenesis could offer a prominent therapeutic effect, supported by viral infection- and cancer-targeting miR therapeutics clinical trials(Rupaimoole & Slack, 2017). Therefore, miR-based therapeutics for hard-to-heal wounds represent a promising approach(Herter & Xu Landen, 2017; Luan et al., 2018; Meng et al., 2018; Nie et al., 2020; Pastar et al., 2021; Sen & Roy, 2012).

However, our insufficient knowledge of the miR-mediated gene regulation in human wounds severely hinders the identification of clinically relevant miRs and their potential therapeutic use. While most previous wound healing-related miR studies rely on *in vitro* or animal models, only a few have approached miR profiles in human wound tissues or primary cells from patients, including tissues and fibroblasts of diabetic foot ulcers(Liang et al., 2016; Ramirez et al., 2018), burn wound dermis(Liang et al., 2012), and acute wounds at the inflammatory phase(Li et al., 2015). Despite sharing several fundamental features, the human skin structure and repair processes are different from those of the commonly used animal models (e.g., rodents)(Elliot et al., 2018). Moreover, animal models cannot fully

simulate the human disease complexity, and the findings are difficult to extrapolate to humans(Darwin & Tomic-Canic, 2018; Pastar et al., 2018). Thereby, a rigorous and in-depth characterization of miR-mediated gene regulatory networks in human healing and non-healing wounds is timely needed.

In this study, we performed paired small and mRNA expression profiling in the human skin, acute wounds during the inflammatory and proliferative phases, and VU, unraveling time-resolved changes of the whole transcriptome throughout the wound healing process and the unique gene expression signature of a common chronic wound type. The integrative miR and mRNA omics analysis provides a network view of miR-mediated gene regulation in human wounds *in vivo* and demonstrates the functional involvement of miRs in human skin wound repair at the system level. Importantly, we identified miRs highly relevant to VU pathology, based not only on their aberrant expression but also their targetome enriched in the VU-related gene expression signature. Apart from confirming the *in silico* findings, the experimental miR expression, targetome, and function validation uncovered that VU-dysregulated miRs could act cooperatively contributing to the stalled wound healing characterized by failed transition from inflammatory-to-proliferative phase, which opens up new possibility for the development of more precise and innovative wound treatment targeting pathologically-relevant cooperating miRs to achieve higher therapeutic efficacy and specificity. Additionally, based on this comprehensive analysis of human wound tissues, we built a browsable resource web portal (https://www.xulandenlab.com/humanwounds-mirna-mrna), which is the first wound healing-focused miR resource for facilitating the exploration of miR's clinical application and for aiding in the elucidation of posttranscriptional regulatory underpinnings of tissue repair.

Materials and Methods

Human wound samples

Human wound biopsies were obtained from 10 healthy donors and 12 patients with chronic venous ulcer (VU) at the Karolinska University Hospital Solna (Stockholm, Sweden). Donor demographics are presented in Table S1. Patients with VUs, which persisted for more than four months despite conventional therapy, were enrolled in this study (Table S2). Tissue samples were collected from the lower extremity at the nonhealing edges of the ulcers by using a four-mm biopsy punch (Fig. 1a). Healthy donors above 60 years old without skin diseases, diabetes, unstable heart disease, infections, bleeding disorder, immune suppression, and any ongoing medical treatments were recruited (Table S3).

103 Two full-thickness excisional wounds (4 mm in diameter) were created at the lower extremity on each
104 donor, and the excised skin was saved as intact skin control (Skin). The wound-edges were excised
105 with a six mm-biopsy punch at day one (Wound1) and day seven (Wound7) after wounding (Fig. 1a).
106 Written informed consent was obtained from all the donors to collect and use the tissue samples. The
107 study was approved by the Stockholm Regional Ethics Committee and conducted according to the
108 Declaration of Helsinki's principles.

109 **RNA extraction, library preparation, and sequencing**

110 *RNA extraction* Snap frozen tissue samples were homogenized with the TissueLyser LT (Qiagen), and
111 total RNA was isolated using the miRNeasy Mini kit (Qiagen). RNA quality and quantity were determined
112 by using Agilent 2100 Bioanalyzer (Agilent Technologies) and Nanodrop 1000 (Thermo Fisher Scientific
113 Inc.), respectively.
114
115 *Small RNA library preparation and sequencing* The small RNA sequencing libraries were constructed
116 using 3 µg total RNA per sample and NEB Next® Multiplex Small RNA Library Prep Set for Illumina®
117 (NEB) following the manufacturer's recommendation. Briefly, total RNA was first ligated to adaptors at
118 the 3' end by NEB 3' SR adaptor and 5' end by T4 RNA ligase followed by reverse transcription into
119 cDNA using M-MuLV Reverse Transcriptase. PCR amplification of cDNA was performed using SR
120 primers for Illumina and index primers. The PCR products were purified, and DNA fragments spanning
121 from 140 to 160bp were recovered and quantified by DNA High Sensitivity Chips on the Agilent
122 Bioanalyzer. The libraries were sequenced on an Illumina Hiseq 2500 platform (Illumina, Inc.) using
123 single-end 50bp reads, and all samples were run side by side.
124
125 *mRNA library preparation and sequencing* The long RNA sequencing libraries were constructed with a
126 total amount of 2 µg RNA per sample. First, the ribosomal RNA was depleted by Epicentre Ribo-zero®
127 rRNA Removal Kit (Epicentre). Second, strand-specific total-transcriptome RNA sequencing libraries
128 were prepared by incorporating dUTPs in the second-strand synthesis step with NEB Next® Ultra™
129 Directional RNA Library Prep Kit for Illumina® (NEB). Finally, the libraries were sequenced on an
130 Illumina Hiseq 4000 platform, and 150 bp paired-end reads were generated for the following analysis.

131

132 **Analysis of miRNA-sequencing data**

133 *Quality control, mapping, and quantification* Quality of raw data was assessed using FastQC v0.11.8
134 (http://www.bioinformatics.babraham.ac.uk/projects/fastqc/). We used mapper.pl module in the
135 miRDeep2 v0.1.3 package(Friedlander et al., 2012; Mackowiak, 2011) to filter low-quality reads and
136 remove sequencing adaptors and redundancies. Trimmed reads with lengths greater than 18
137 nucleotides were mapped to GENCODE human reference genome (hg38) by the software Bowtie
138 v1.2.2(Langmead et al., 2009). The miRDeep2.pl module was then performed with default parameters
139 to identify known miRNAs, which were compared to miRNAs in miRBase release 22.1(Kozomara et al.,
140 2018). Counts of reads mapped to each known mature miRNAs were acquired from the quantifier.pl
141 module output without allowing mismatch. miRNAs with read counts less than five in more than half of
142 twenty samples were discarded since these miRNAs are unlikely to give stable and robust results. Raw
143 counts of 562 miRNAs were normalized for sequencing depth using TPM methods (transcript per million
144 = mapped read count/total reads * 10e6)(Zhou et al., 2010) and prepared for further analysis.

145 *Differential expression (DE) analysis* The DESeq2 workflow(Love et al., 2014) was carried out to fit raw
146 counts to the negative binomial (NB) generalized linear model and to calculate the statistical
147 significance of each miRNA in each comparison. In particular, the paired model was employed when
148 comparing samples from the same donor. *P-value*s obtained from the Wald test were corrected using
149 Benjamini-Hochberg (BH) multiple test to estimate the false discovery rate (FDR). The differentially
150 expressed miRNAs were defined as FDR < 0.05 and |log2(fold change)| ≥ 1.

151 *Principal component analysis (PCA)* To explore the similarity of each sample, PCA was performed by
152 using a DESeq2 built-in function *plotPCA* on the transformed data, in which the variances and size
153 factors were stabilized and corrected. PCA and heatmaps were plotted by using *ggplot2*(Hadley, 2016)
154 and *ComplexHeatmap*(Gu et al., 2016) packages in RStudio (https://rstudio.com/).

155 *Weighted gene co-expression network analysis (WGCNA)* The normalized expression of 562 miRNAs
156 were used as input to the WGCNA R package(Langfelder & Horvath, 2008). First, we calculated the
157 strength of pairwise correlations between miRNAs using the 'biweight' mid-correlation method. The
158 function *pickSoftThreshold* was then employed to compute the optimized soft-thresholding power based
159 on connectivity, which led to an approximately scale-free network topology(Zhang & Horvath, 2005).
160 Second, a signed weighted co-expression network was constructed with a power of 18 using the one-

161 step *blockwiseModules* algorithm (Fig. S2a). Network modules were filtered according to parameters:
162 *minModuleSize* = 10 and *mergeCutHeight* = 0.25.
163 The expression profile of each module was represented by the module eigengene (ME), referred to as
164 the first principal component of all miRNAs in each module. Pearson correlations (values from -1 to 1)
165 and the corresponding *P-value*s between MEs and traits were computed. *P-value*s were further
166 adjusted to FDR across all the modules using the BH method. Modules significantly associated with
167 each trait were selected by FDR < 0.05 and absolute correlation coefficients > 0.4. The module
168 membership (also known as kME) of each miRNA was calculated by the correlations between miRNA
169 expression and ME. MiRNAs with the highest kME values were defined as intra-modular hub miRNAs,
170 and networks of hub miRNAs in significant modules were visualized using the Cytoscape v3.7.2
171 software(Shannon et al., 2003).
172 To check the robustness of module definition, we carried out module preservation analysis and
173 calculated the standardized Z-scores for each module by permutating 200 times using the same 20
174 samples as reference and test datasets. Modular preservation is strong if Z-summary > 10, weak to
175 moderate if 2 < Z-summary < 10, no evidence of preservation if Z-summary ≤ 2(Langfelder et al., 2011).

176 *Transcription factor (TF) enrichment analysis* We leveraged a curated database about TF-miRNA
177 regulations, TransmiR v2.0(Tong et al., 2019), to identify the TFs regulating miRNA expression in each
178 module. Fisher's exact tests were employed to evaluate the enrichment of each TF in the significant
179 modules, and FDRs were adjusted to the total number of TFs (Odds ratio > 1 and FDR < 0.05).
180 Correlations of gene expression between TFs and miRNA modules (represented by MEs) were further
181 filtered to identify putative TF-mediated miRNA gene expression patterns (Pearson correlation: *P-value*
182 < 0.05, coefficient > 0). The 562 miRNAs abundantly expressed in our samples were treated as the
183 background dataset.

184

185 **Analysis of mRNA sequencing data**

186 Raw reads of mRNA sequencing were first trimmed for adaptors and low-quality bases using
187 Trimmomatic v0.36 software(Bolger et al., 2014). Clean reads were aligned to the human reference
188 genome (GRCh38.p12), coupled with the comprehensive gene annotation file (GENCODEv31) using
189 STAR v2.7.1a(Dobin et al., 2013). Gene expression was then quantified by counting unique mapped

190 fragments to exons by using the feature count function from the Subread package(Liao et al., 2013).
191 Raw counts for each gene were normalized to fragments per kilobase of a transcript, per million mapped
192 reads (FPKM)-like values. Only mRNAs with FPKM ≥ 1 in at least ten samples were kept for the rest
193 analysis. We used the same pipeline described above for mRNA DE and PCA analysis. The
194 differentially expressed mRNAs were defined as FDR < 0.05 and |log2(fold change)| ≥ 0.58. WGCNA
195 was carried out for 12,069 mRNAs with the optimal threshold power of 12 according to a fit to the scale-
196 free topology of the co-expression network (Fig. S4a). Thirteen mRNA modules were identified with the
197 settings: *maxBlockSize* = 20000, *minModuleSize* = 100 and *mergeCutHeight* = 0.25. Furthermore,
198 mRNA module-enriched TF analysis was performed with a manually curated TF-target regulatory
199 relationship database, TRRUST v2(Han et al., 2018), using Fisher's exact tests. TFs with FDR < 0.05
200 and odds ratio > 1 and the expression significantly correlated with respective mRNA modules (Pearson
201 correlation *P-value* < 0.05) were identified.

202 *Gene ontology (GO) analysis* We carried out GO analysis for mRNAs by using the WebGestalt tool
203 (http://www.webgestalt.org/)(Liao et al., 2019), which applied a hypergeometric test in target and
204 reference gene sets. GO terms of non-redundant biological process (BP) with gene number less than
205 10 and adjust *P- value* (FDR) > 0.05 were filtered out.
206

207 **Integrative analysis of miRNA and mRNA expression changes in wound healing**

208 *Expression correlation between mRNA and miRNA modules* An integrative analysis was carried out by
209 relating the first principal component (PC1) of miRNA expression, calculated using the
210 *moduleEigengenes* function of WGCNA package(Langfelder & Horvath, 2008), to the PC1 of mRNA
211 expression in each module. The miRNA-mRNA module pairs with a Pearson correlation coefficient < -
212 0.5 and a *P-value* < 0.05 were selected for the following enrichment analysis.

213 *Prediction of miRNA targets* We predicted both conserved and non-conserved target sites for all the
214 562 miRNAs by using the *get_multimir* function from R package multimiR(Ru et al., 2014)
215 (http://multimir.org/) based on the latest TargetScan v7.2 database(Agarwal et al., 2015; Lewis et al.,
216 2005). All predicted miRNA targets were sorted by a primary score calculated for target site strength,

217 and the top 25% with summed context++ score ≤ -0.15 were defined as the strongest miRNA targets.
218 Targets that were not detected by the long RNA-seq were removed.

219 *Gene set enrichment analysis of miRNA targets in mRNA modules.* We evaluated the degree of
220 enrichment of miRNA modules' targets in mRNA modules. For this, we focused on the VU-specific DE
221 miRNA, i.e., the 22 up- and 10 down-regulated miRNAs in VU compared to both the skin and acute
222 wounds (FDR < 0.05 and |log2(fold change)| ≥ 1), as well as the VU-associated modules' hub miRNAs,
223 which kME values were greater than the median kME in respective modules (i.e., 14 miRNAs in m8, 9
224 miRNAs in m12, 20 miRNAs in m7, 29 miRNAs in m3, and 13 miRNAs in m9). Among these miRNAs'
225 strongest targets, we selected the ones that were hit by ≥ 2 miRNAs from m8, m9, m12 modules or
226 miRNAs downregulated in VU; ≥ 3 miRNAs from m7 module or miRNAs upregulated in VU; ≥ 4 miRNAs
227 from m3 module, to capture putative module-driving targets. We performed gene set enrichment
228 analyses for these miRs' targets in VU-specific DE mRNAs (FDR < 0.05 and fold change ≥ 1.5) and
229 VU-associated mRNA modules by using the R function *fisher.test()* based on the two-side Fisher's exact
230 test(Wu et al., 2016). Furthermore, we performed enrichment analysis to identify individual miRNA with
231 their strongest targets significantly enriched in VU-specific DE mRNAs or VU-associated mRNA
232 modules (Fisher's exact test: odds ratio > 1, *P-value* < 0.05).
233

234 **Experimental validation of miRs' expression, targetome, and functions**

235 *Quantitative RT-PCR* To detect miRNA, RNA from human skin and wounds was reverse transcribed
236 using TaqMan® Advanced miRNA cDNA Synthesis Kit (Thermo Fisher Scientific). Individual miRNA
237 expression was then quantified using TaqMan® Advanced miRNA Assays (Thermo Fisher Scientific)
238 and normalized with miR-361-5p and miR-423-5p due to their relatively constant expression between
239 human skin and wounds. To detect mRNA, we performed reverse transcription using the RevertAid
240 First Strand cDNA Synthesis Kit (ThermoFisher Scientific). Gene expression was examined by SYBR
241 Green expression assays (ThermoFisher Scientific) and normalized with housekeeping gene B2M and
242 GAPDH. The primer sequences for B2M are forward primer (5'-AAGTGGGATCGAGACATGTAAG-3')
243 and reverse primer (5'-GGAGACAGCACTCAAAGTAGAA-3'); GAPDH forward primer (5'-
244 GGTGTGAACCATGAGAAGTATGA-3') and reverse primer (5'-GAGTCCTTCCACGATACCAAAG-3').

245 *Primary cell culture and transfection* Adult human epidermal keratinocytes were cultured in EpiLife
246 serum-free keratinocyte growth medium supplemented with Human Keratinocyte Growth Supplement
247 (HKGS) and 100 units/mL Penicillin and 100 µg/mL Streptomycin (Thermo Fisher Scientific). Adult
248 human dermal fibroblasts were cultured in Medium 106 supplemented with Low Serum Growth
249 Supplement (LSGS) and 100 units/mL Penicillin and 100 µg/mL Streptomycin (Thermo Fisher Scientific).
250 Cells were incubated at 37°C in 5% CO_2, and media was routinely changed every 2–3 days. Third
251 passage keratinocytes at 50%-60% confluence were transfected with 20 nM miRNA mimics (Horizon)
252 or negative control using Lipofectamine™ 3000 (Thermo Fisher Scientific).

253 *Microarray analysis* Transcriptome profiling of keratinocytes and fibroblasts transfected with 20 nM
254 miRNA mimics or control mimics for 24 hours (in triplicates) was performed using Affymetrix Genechip
255 system at the Microarray Core facility of Karolinska Institute. Normalized expression data (log2
256 transformed value) were exported from Transcriptome Analysis Console (TAC) software and analyzed
257 by the *limma* R package(Ritchie et al., 2015). In brief, expression data were first fitted to a linear model
258 for each probe. Then, the empirical Bayes method was applied to compute the estimated coefficients
259 of gene-wise variability and standard errors for comparisons of experimental and control groups. Genes
260 with FC > 1.2 and *P*-value < 0.05 between the miRNA mimics- and the control mimics-transfected cells
261 were considered to be significantly changed. Gene set enrichment analysis, including biological process
262 (BP), Kyoto Encyclopedia of Genes and Genomes (KEGG) pathway, and hallmark from Molecular
263 Signatures Database (MSigDB) (http://www.gsea-msigdb.org/)(Subramanian et al., 2005), was
264 performed with a ranked fold change list of all the genes by using the *fgsea* R package(Korotkevich et
265 al., 2021) and visualized by using the *ggplot2*(Hadley, 2016) and *circlize*(Gu et al., 2014) packages.

266 *Immunofluorescence staining* Cells transfected with a combination of miRNA and/or control mimics (50
267 nM in total) were fixed in 4% paraformaldehyde (PFA) for 15 minutes. Cells were incubated with the Ki-
268 67 antibody (Cell Signaling Technology) overnight at 4°C. The next day, cells were incubated with the
269 secondary antibody conjugated with Alexa 488 for 40 minutes at room temperature. Cells were mounted
270 with the ProLong™ Diamond Antifade Mountant with 4',6-Diamidino-2-Phenylindole (DAPI)
271 (ThermoFisher Scientific). Ki-67 signals were visualized with Nikon microscopy, and positive cells were
272 counted using ImageJ software (National Institutes of Health).

273 *Cell proliferation assay* Cells were seeded in 12-well plates with a density of 20,000 cells/well. The
274 plates were placed in IncuCyte live-cell imaging and analysis platform (Essen Bioscience) after cells

275 attaching to the plates. Plates were imaged every two hours, and pictures were processed and analyzed
276 using IncuCyte ZOOM 2018A software (Essen Bioscience).

277 *Statistical analysis* Sample size of each experiment is indicated in the figure legend. Data analysis was
278 performed by using R and Graphpad Prism 7 software. Comparison between two groups was performed
279 with Mann-Whitney U tests (unpaired, non-parametric), Wilcoxon signed-rank test (paired, non-
280 parametric), or two-tailed Student's t-test (parametric). The cell growth assay was analyzed by using
281 two-way ANOVA. P-value < 0.05 is considered to be statistically significant.

282

283 **Results**

284 **miRNA and mRNA paired expression profiling in human wounds**

285 To better understand tissue repair in humans, we collected wound-edge tissues from human acute
286 wounds and chronic non-healing VUs (Fig. 1a and Table S1–S3). We created 4mm full thickness punch
287 wounds at the lower legs of healthy volunteers aged beyond 60 years to match the advanced age of
288 VU patients and anatomical location of the highest VUs occurrence(Vivas et al., 2016). Tissue was
289 collected at baseline (Skin), and at day one and day seven post-wounding (Wound1 and Wound7) to
290 capture the inflammatory and proliferative phases of wound healing, respectively. In total, 20 samples
291 divided into four groups, i.e., Skin, Wound1, Wound7, and VU, were analyzed by Illumina small RNA
292 sequencing (sRNA-seq) and ribosomal RNA-depleted long RNA sequencing (RNA-seq). After stringent
293 raw sequencing data quality control (Table S4–S5), we detected 562 mature miRs and 12,069 mRNAs
294 in our samples. Our principal component analysis showed that either the miR or the mRNA expression
295 profiles clearly separated these four sample groups (Fig. 1b). Next, we performed pairwise comparisons
296 to identify the differentially expressed genes (DEG) during wound repair. We compared the VUs with
297 both the skin and acute wounds and unraveled a VU-specific gene signature, including aberrant
298 increase of 22 miRs and 221 mRNAs and decrease of 10 miRs and 203 mRNAs (DE analysis
299 FDR < 0.05, fold change ≥ 2 for miRs and ≥ 1.5 for mRNAs, Fig. 1c–e and Additional file 1). The full
300 DEG list can be browsed on our resource website (https://www.xulandenlab.com/humanwounds-mirna-
301 mrna) with more or less rigorous cut-offs. With this unique resource, we dissected further the miR-
302 mediated posttranscriptional regulatory underpinnings of wound repair.

303

304 **Dynamically changed miR expression during wound repair**

305 We leveraged weighted gene co-expression network analysis (WGCNA) for classifying miRs according
306 to their co-expression patterns in the 20 sRNA-seq-analyzed samples to link the miR expression
307 changes with wound healing progression or non-healing status at a system level(Langfelder & Horvath,
308 2008). We identified 13 distinct modules with a robustness confirmed by the module preservation
309 analysis (Fig. S1a), ten of them significantly correlating (Pearson's correlation, FDR < 0.05) with at least
310 one of the four phenotypic traits, i.e., Skin, Wound1, Wound7, and VU (Fig. 2a and b, Additional file 2).
311 The WGCNA revealed that module (m)2, m10, and m11 miRs were upregulated at the inflammatory

312 phase (Wound1), while m5 and m6 miRs peaked at the proliferative phase (Wound7). In VU, we
313 identified three downregulated (m3, m7, and m9) and two upregulated (m8 and m12) miR modules. We
314 highlighted the 198 “driver” miRs (i.e, the top 20 miRNAs with the highest kME values in each module
315 and kME > 0.5) of the ten significant modules in the co-expression networks (Fig. 2c, d and Fig. S2b–i)
316 and they could also be browsed on our resource web portal
317 (https://www.xulandenlab.com/humanwounds-mirna-mrna). Notably, we identified 84% of them as
318 DEGs, suggesting a high consistence between the WGCNA and DE analysis (Additional file 3).
319

320 We hypothesized that the co-expression of various miRs could be due to their transcription driven by
321 common transcription factors (TF). To test this idea, we leveraged TransmiR v2.0(Tong et al., 2019), a
322 database including literature-curated and ChIP-seq-derived TF-miR regulation data, to identify the
323 enriched TFs in each miR module [Fisher’s extract test: odds ratio (OR) > 1, *FDR* < 0.05, Additional file
324 4]. Interestingly, the BMP4, KLF4, KLF5, GATA3, GRHL2, and TP53 families exhibited not only their
325 binding sites enriched in the m9 miR genes but their expression also significantly correlated with the
326 m9 miRs (Pearson’s correlation coefficient = 0.53–0.82, *P*-value of *p* = 7.05e-06–0.014) (Fig. 2d, Fig.
327 S3a and Additional file 4). Notably, the BMP4, GATA3, and KLF4 expressions were significantly
328 reduced in VU compared to the skin and acute wounds. This result could explain the deficiency of their
329 regulated miRs in VU and also suggest a link between these TFs and chronic wound pathology (Fig.
330 S3b).
331

332 **mRNA co-expression networks underpinning wound repair**

333 miRs exert functions through the posttranscriptional regulation of their target mRNAs. Therefore,
334 describing the mRNA expression context would be required for understanding the role of miRs in wound
335 repair(Agarwal et al., 2015). We thus performed WGCNA in the paired long RNA-seq data and identified
336 13 mRNA co-expression modules (Fig. 2e, Fig. S1b and 4a–c, and Additional file 5). The GO analysis
337 of the mRNA modules largely confirmed the previous knowledge of wound biology, such as skin
338 hemostasis (M2) and barrier function (M4)-related gene downregulation in the wounds, the upregulation
339 of the genes involved in the immune response (M8), RNA processing, and protein production (M1, M3,
340 and M5) in the inflammatory phase, and the prominent cell mitosis-related gene expression (M7) in the
341 proliferative phase of wound repair (Fig. 2f and Fig. S5a). These results further supported the

342 robustness and reproducibility of our profiling data. Moreover, this unique dataset allows the
343 identification of the key TFs driving these biological processes. For example, we identified NFKB1 and
344 RELA, well-known for their immune functions(Liu et al., 2017), as the most enriched upstream
345 regulators for the M1 mRNAs, while E2F1, a TF promoting cell growth(Ertosun et al., 2016), surfaced
346 as a master regulator TF in M7 (Additional file 6).
347
348 Importantly, our study unraveled a VU molecular signature: downregulated expression of RNA and
349 protein production- (M1, M3, and M5) as well as cell mitosis-related (M7) genes, and upregulated
350 expression of genes involved in extracellular matrix organization and cell adhesion (M9). These results
351 were in line with the dermal tissue fibrosis observed in patients with chronic venous
352 insufficiency(Blumberg et al., 2012; Pappas et al., 1999; Stone et al., 2020). Moreover, we found an
353 immune gene signature clearly distinguishing the chronic inflammation in VUs (M11 and M12 enriched
354 with adaptive immunity-related mRNAs) from the self-limiting immune response in acute wounds (M8
355 enriched with neutrophil activation- and phagocytosis-related mRNAs) (Fig. 2f and Fig. S5b). Overall,
356 we generated a gene expression map of human healing and non-healing wounds, setting a stepping
357 stone for the in-depth understanding of the VU pathological mechanisms. After having established this
358 map, we decided to dissect how miRs contribute to these pathological changes.
359
360 **Integrative analysis of miR and mRNA expression changes in wound healing**
361 Among the multiple gene expression regulatory mechanisms, we aimed to evaluate how miRs could
362 contribute to the protein-coding gene expression in human wound repair. We thus performed a
363 correlation analysis for the miRs and mRNAs that were differentially expressed in VU compared to the
364 skin and acute wounds, using the first principal component (PC1) of their expression in each sample.
365 We found significantly negative correlations (Pearson's correlation, P-values: 1.36e-12–1.27e-04)
366 between the PC1 of the DE miRs and the DE mRNAs predicted as miR targets, indicating negative
367 regulation of VU-mRNA signature by the aberrantly expressed miRs in VU (Fig. 3a–c).
368 Furthermore, we dissected the potential regulatory relationship between the VU-associated miR and
369 mRNA modules. We identified significantly negative correlations between the downregulated miR (m3,
370 m7, and m9) and the upregulated mRNA (M9, M11, and M12) modules, as well as between the
371 upregulated miR (m8 and m12) and the downregulated mRNA (M5) modules in VU (Fig. 3d). Among

372 these miR-mRNA module pairs, we found that the predicted targets of the downregulated m9 miRs
373 were significantly enriched (Fisher's extract test: OR > 1, *P*-value < 0.05) for the upregulated M9
374 mRNAs, whereas the targets of the upregulated miRs and m8 miRs were enriched for the
375 downregulated mRNAs and M5 mRNAs (Fig. 4a and Additional file 7). These results demonstrated that
376 miRs significantly contribute to the aberrant mRNA expression in VU at a global level.
377 Based on the above-identified miR-mRNA module pairs, we next searched for individual candidate miRs
378 with their targets enriched for the VU mRNA signature. We observed that the targets of two VU-
379 associated downregulated miRs (miR-144-3p and miR-218-5p) and five m9 miRs (miR-205-5p, miR-
380 211-5p, miR-506-3p, miR-509-3p, and miR-96-5p) were enriched for the upregulated M9 mRNAs,
381 whereas the targets of three VU-associated upregulated miRs (miR-450-5p, miR-512-3p, and miR-
382 516b-5p) and seven m8 miRs (miR-424-5p, miR-34a-5p, miR-34c-5p, miR-516a-5p, miR-517a-3p, miR-
383 517b-3p, and miR-7704) were enriched for M5 mRNAs and downregulated mRNAs (Fig. 4b and
384 Additional file 8). These miR targetomes were enriched for the mRNAs associated with VU pathology.
385 Therefore, these miR candidates are of importance for understanding the pathological mechanisms
386 hindering wound healing. Moreover, we compiled miR-mediated gene expression regulation networks
387 centered with these highly pathologically relevant miRs (Fig. 4c, FigS6–S7, and Additional file 8). These
388 networks also include the mRNAs predicted as the strongest targets and with anti-correlated expression
389 patterns with these miRs in human wounds *in vivo*, as well as the TFs reported to regulate these miR
390 expressions from the TransmiR v2 database(Tong et al., 2019). Taken together, our study identifies a
391 list of highly pathological relevant miRs and their targetomes in human VU.
392
393 **Experimental validation of miR expressions and targets in human skin wounds**
394 We selected nine shortlisted DE miRs (Fig. 1d and 4b), including three downregulated (miR-149-5p,
395 miR-218-5p, and miR-96-5p) and six upregulated (miR-7704, miR-424-5p, miR-31-3p, miR-450-5p,
396 miR-516b-5p, and miR-517b-3p) miRs in VU, and validated their expression by qRT-PCR in a cohort
397 with seven healthy donors and twelve VU patients, matched in terms of age and the anatomical wound
398 locations (Table S2–S3). We confirmed their expression patterns in RNA-seq, supporting the
399 robustness and reproducibility of our profiling data (Fig. 5a–i and Fig. S8).
400 Furthermore, we experimentally validated the targets of eight miRs surfaced in our analysis (Fig. 4b),
401 including the miRs downregulated (miR-218-5p and miR-96-5p) and upregulated (miR-424-5p, miR-

402 450-5p, miR-516b-5p, miR-34a-5p, miR-34c-5p, and miR-7704) in VU. We performed genome-wide
403 microarray analysis in human primary keratinocytes or fibroblasts overexpressing each of these miRs.
404 Furthermore, we re-analyzed our published microarray dataset on keratinocytes with miR-34a-5p or
405 miR-34c-5p overexpression (GSE117506)(Pachera et al., 2020). For all these eight miRs, we observed
406 that their strongest targets predicted by TargetScan were significantly downregulated compared to the
407 non-targeting mRNAs (Wilcoxon t-test P-values: 1.34e-25~1.91e-59). The differences were more
408 significant when we divided the strongest targets into conserved and experimentally validated subtypes,
409 confirming the bioinformatics prediction robustness of the miR targets applied in this study (Fig. 5j–m
410 and Fig. S9a–i).

411 Notably, we observed significant enrichment (Fisher's exact test, OR > 1, *P*-value < 0.05) of the
412 experimentally validated miR-218-5p, miR-34a-5p, miR-34c-5p, and miR-7704 targets for the VU gene
413 signature (Fig. 5n and Additional file 9). We have previously shown that miR-34a and miR-34c inhibit
414 keratinocyte proliferation and migration, while promoting apoptosis and inflammatory response,
415 resulting in delayed wound repair in a mouse model(Pachera et al., 2020). We validated robustness of
416 the bioinformatics approach applied in this study by miR-34a/c re-identification. Here, we discovered
417 that both the predicted (Fig. 4b) and validated (Fig. 5n) miR-34a/c targets were enriched for the
418 downregulated M5 module mRNAs in VU. Notably, our microarray analysis confirmed that miR-34a/c
419 reduced the expression of 39 hub genes in the M5 module [log2(fold change) ≤ -0.58, *P*-value < 0.05,
420 Fig. S9j], and 26 of them exhibited negative correlation (Pearson's $r = -0.83 – -0.45$, *P*-value < 0.05)
421 with miR-34a/c expression levels in the human skin and wound samples (Fig. 5o and Additional file 9),
422 suggesting that they were miR-34a/c targets *in vivo*. MiR-218-5p was downregulated in the VU
423 compared to the acute wounds and the skin (Fig. 5b and Fig. S8). Its predicted (Fig. 4b) and validated
424 (Fig. 5n) targets were both enriched for the upregulated or M9 module mRNAs in VU. Among the ten
425 *in vitro* validated targets, eight negatively correlated (Pearson's $r = -0.82 \sim -0.46$, *P*-value of $p < 0.05$)
426 with miR-218-5p expression in the human skin and wounds (Fig. 5o, Fig. S9j, and Additional file 9).
427 Interestingly, this study also identified miR-7704, a human-specific miR, with significantly increased
428 expression in VU (Fig. 5d and Fig. S8). Similar to miR-34a/c, the predicted (Fig. 4b) and validated
429 (Fig. 5n) miR-7704 targets were highly enriched for the M5 module mRNAs downregulated in VU.

430 For miR-96-5p, miR-424-5p, miR-450-5p, and miR-516b-5p, although their predicted targets were
431 significantly enriched (Fisher's exact test: OR > 1, *P*-value < 0.05) for VU-associated mRNAs (Fig. 4b),

432 we did not find similar enrichment for their experimentally validated targets. Nevertheless, these miRs
433 regulated some VU-associated hub genes *in vitro* (Fig. S9k) and also exhibited an anti-correlated
434 expression pattern with their targets *in vivo* (Fig. 5p), e.g., miR-96-5p from the downregulated m9
435 module targets the M9 mRNAs upregulated in VU, including TP53INP1, LAMC1, EDNRA, GJC1, and
436 FN1; while miR-424-5p from the upregulated m8 miR module targets the M5 mRNAs downregulated in
437 VU, including SLC25A22, VPS4A, and GHR (Additional file 9).

438 In summary, we experimentally validated the expression and targets of the miRs identified by the RNA-
439 seq data bioinformatics analysis, confirming the robustness and reproducibility of this dataset and
440 highlighting its value as a reference for studying the physiological and pathological roles of miRs in
441 human skin wound healing.

442

443 **Cooperativity of VU pathology-relevant miRs**

444 From the miR-mediated gene expression regulation networks underpinning VU pathology (Fig. S6–S7
445 and Additional file 8), we caught a glimpse of presumable miR cooperativity through targeting the same
446 mRNAs, i.e., co-targeting among miRs, which reportedly imposing stronger and more complex
447 repression patterns on target mRNA expression(Cherone et al., 2019). For the miRs with unrelated
448 seed sequences, we found that miR-34a/c and miR-424-5p or miR-7704 shared eight–ten targets, and
449 these miRs were co-expressed in the m8 module. We showed that among the downregulated miRs in
450 VU, miR-96-5p and miR-218-5p shared eight targets.
451 In addition, we performed functional annotations for the genes regulated by the VU-associated miRs
452 identified in the microarray analysis (Fig. 6a and Additional file 10). Both miR-218-5p and miR-96-5p
453 promoted ribosome biogenesis and non-coding (nc) RNA processing, while miR-218-5p also
454 suppressed keratinization. miR-34a/c-5p enhanced innate immune response, while reducing mitosis.
455 Similarly, miR-424-5p and miR-516b-5p increased the cellular defense response, while inhibiting cell
456 proliferation. In addition, we showed that miR-450-5p upregulated genes related to the ncRNA
457 metabolic process and mitochondrial respiratory chain complex assembly, whereas miR-7704
458 downregulated insulin, ERBB, and small GTPase-mediated signaling pathway-related genes. Of
459 particular interest, combining the miR expression changes with their annotated functions, we found a
460 regular pattern, i.e., the miRs upregulated in VU (i.e., miR-34a-5p, miR-34c-5p, miR-424-5p, miR-450-
461 5p, miR-7704, and miR-516-5p) promoted inflammation but inhibited proliferation; whereas the miRs

462 downregulated in VU (i.e., miR-218-5p and miR-96-5p) were required for cell growth and activation
463 (Fig. 6b). Therefore, these VU-dysregulated miRs might cooperatively contribute to the stalled wound
464 healing characterized with failed transition from inflammation-to-proliferation(Landen et al., 2016).
465

466 **Cooperation of miR-34a, miR-424, and miR-516 in regulating keratinocyte proliferation and**
467 **inflammatory response**

468 To validate miR cooperativity in modulating the key pathological processes in VU, we analyzed
469 proliferation and inflammatory response of keratinocytes overexpressing individual miR or miR
470 combinations. The microarray data gene ontology analysis (Fig. 6b) showed that three miRs
471 upregulated in VU could suppress the expression of mitotic spindle-related genes (Fig. 6c): miR-34a/c-
472 5p reduced the level of 41 mRNAs (including two miR-34a/c targets), while miR-424-5p downregulated
473 the expression of 67 mRNAs (including 14 miR-424 targets). Although 33 mRNAs were commonly
474 regulated by miR-34a/c-5p and miR-424-5p, none of them were co-targeted by these miRs (Fig. 6c).
475 Similarly, in the cell cycle pathway, miR-34a-5p directly targeted CCND1, CDK6, HDAC1, and E2F3,
476 while miR-424-5p targeted ANAPC13, CCNE1, CDC25B, CDK1, CDKN1B, CHK1, WEE1, and YWHAH,
477 and only CDC23 was co-targeted by both miRs (Fig. 7a). We thus hypothesized that miR-34a-5p and
478 miR-424-5p might cooperate to impact stronger on cell proliferation by targeting different gene sets
479 within the same signaling pathway. To test this idea, we measured keratinocyte growth by detecting
480 proliferation marker gene Ki67 expression both on mRNA and protein levels. We found that although
481 miR-34a-5p or miR-424-5p alone could reduce Ki67 levels, their combination suppressed stronger Ki67
482 expression (Fig. 7b–c and Fig. S10a). The cooperativity between miR-34a-5p and miR-424-5p in
483 repressing keratinocyte growth was further confirmed by comparing cell growth curves generated with
484 a live cell imaging system (Fig. 7d, Fig. S10b and Additional file 11). Moreover, our microarray analysis
485 showed that the miR-34a-5p and miR-516b-5p combination extended the list of inflammatory response-
486 related upregulated genes (Fig. 6d). In line with this, simultaneously overexpressing miR-34a-5p and
487 miR-516b-5p induced a higher inflammatory chemokine CCL20 expression compared to the individual
488 overexpression of each miRNA (Fig. 7e). In summary, our study identified VU signature miRs, e.g.,
489 miR-34a, miR-424, and miR-516, with cooperativity in inflicting more severe pathological changes
490 (Fig. 7f). These findings open new opportunities of developing wound treatment targeting cooperating
491 miRs with potentially higher therapeutic efficacy and specificity.

492 **Discussion**

493 Our genome-wide paired analysis of miR and mRNA expression in human healing and non-healing
494 wounds provides a novel global landscape of the miR regulatory roles in wound biology. A detailed
495 overview of the mRNA expression context at different healing stages or under pathological condition
496 VU allows a more precise understanding about the complex role of miRs in wound repair. The same
497 miR is often described to play different or even opposite roles in different cells, as each cell type has
498 specific gene expression context subjected to the miR-mediated posttranscriptional regulation(Erhard
499 et al., 2014). Thereby, the different mRNA expression profiles in acute or chronic wounds should be
500 considered to understand the precise role of an miR in these distinct contexts. With this aspect in mind,
501 we highlight miRs with their targetome most enriched in the VU mRNA signature, as these miRs display
502 a higher likelihood to regulate pathologically relevant genes. Notably, certain of these miRs did not
503 exhibit the greatest expression change in VU, they would thus be missed with the commonly used
504 strategy that focuses on the top miR expression profiling data changes.

505 Another strength of our study is the decryption of time-resolved miR-mRNA expression pattern during
506 human skin wound healing, providing a temporal view to our understanding of the functional miR roles.
507 miRs and their target gene expression contexts change dynamically to support different functional
508 needs during wound repair. Defining an miR as “pro-healing” or “anti-healing” requires specifying its
509 temporal expression pattern. For example, continuous expression of a miR that is beneficial for one
510 healing phase but not the other might also lead to deleterious effects.

511 To understand the molecular mechanisms underlying the miR co-expression patterns, we analyzed the
512 enriched TFs for each miR module with experimentally validated TF-miR regulation data(Tong et al.,
513 2019). This analysis led us to important TFs, such as BMP4(Botchkarev, 2003; Lewis et al., 2014) and
514 GATA3(Kaufman et al., 2003; Kurek et al., 2007) that play fundamental roles in skin development and
515 postnatal remodeling, as well as KLF4, crucial for establishing skin barrier function(Segre et al., 1999).
516 Notably, both GATA3 and KLF4 are reportedly downregulated in human VU(Stojadinovic et al., 2014;
517 Stojadinovic et al., 2008). Our study confirms these findings and provides a novel insight, showing that
518 the loss of these TFs might contribute to VU pathology through their regulated miRs.

519 Numerous miRs that reportedly regulate wound healing in animal models also surfaced in our study,
520 supporting the robustness of our profiling data and bioinformatics analysis. Thereby, our data would be

521 potentially helpful to evaluate the clinical relevance of these miRs. For example, miR-34a/c reportedly
522 enhance keratinocyte inflammatory response, while suppressing proliferation and migration in cultured
523 cells and mouse wound models(Wu et al., 2020). miR-34a was also identified as one of the most
524 induced miRs in diabetic foot ulcer fibroblasts. Induction of miR-34a together with miR-21-5p and miR-
525 145-5p inhibits fibroblast movement and proliferation, whereas activates cell differentiation and
526 senescence(Liang et al., 2016). In this study, we described that miR-34a/c were specifically upregulated
527 in VU, whereas their levels during wound repair remained relatively low and stable, suggesting their
528 specific role in wound pathology. miR-34 targets were enriched in the M5 mRNA module, containing
529 genes upregulated in the inflammatory phase of wound healing but downregulated in VUs. The VU-
530 relevant miR-34 targetome identified in this study would be potentially useful for determining the precise
531 role of miR-34 in VU pathology. Our current findings in human samples together with previous functional
532 data(Liang et al., 2016; Wu et al., 2020) suggest that miR-34 inhibition along with modulation of
533 additional deregulated miRs might be a promising VU treatment approach.

534 In addition, certain of these VU-related miRs are involved in skin-related functions but have not yet been
535 linked to wound healing. For example, miR-218-5p regulates hair follicle development(Zhao et al., 2019),
536 inhibits melanogenesis(J. Guo et al., 2014), and enhances fibroblast differentiation(F. Guo et al., 2014).
537 miR-7704 was identified as an exosomal miR produced by melanocytes(Shen et al., 2020). miR-424-
538 5p suppresses keratinocyte proliferation(Ichihara et al., 2011) and cutaneous angiogenesis(Nakashima
539 et al., 2010; Yang et al., 2017). Moreover, our VU-related miR list (Fig. 4b) also contains miRs without
540 prior knowledge in their role either in skin or wound healing, e.g., miR-517a-3p, miR-517b-3p, miR-
541 516b-5p, miR-512-3p, and miR-450-5p. It would be highly interesting to examine the role of these miRs
542 in VU. Overall, our dataset can serve as a valuable reference for prioritizing clinically relevant miRs for
543 further functional studies.

544 Moreover, we studied the relationships between the dysregulated miRs in VU, regarding their target
545 repertoire and biological functions and identified miRs that could act cooperatively. Such knowledge is
546 required for developing combined miR therapeutics with increased specificity and efficacy(Lai et al.,
547 2019). In the miR-target networks underpinning VU (Fig. S6–S7), we identified a few putative
548 cooperating miR pairs/clusters that were co-expressed and shared multiple common targets, including
549 the upregulated miR-34a/c together with miR-424-5p and miR-7704, as well as the downregulated miR-
550 218-5p and miR-96-5p in VU. Furthermore, although not sharing targets, the majority of the VU-

551 dysregulated miRs could still regulate the common biological processes coordinately. For example, the
552 miRs upregulated in VU (e.g., miR-34a/c-5p, miR-424-5p, miR-450-5p, miR-7704, and miR-516-5p)
553 promote inflammation but inhibit proliferation; whereas the miRs downregulated in VU (e.g., miR-218-
554 5p and miR-96-5p) are needed for cell growth and activation. As a combined consequence, this VU-
555 miR signature could disrupt the swift transition from inflammation to proliferation (Fig. 7f). The failure of
556 this phase transition represents a core pathology of chronic wounds(Eming et al., 2014; Landen et al.,
557 2016). Our findings open the possibility of developing innovative wound treatment targeting multiple
558 pathologically relevant cooperating miRs to attain higher therapeutic efficacy and specificity.

559 Based on the integrative small and long RNA-omics analysis of human wound tissues, we have
560 developed an openly available compendium (https://www.xulandenlab.com/humanwounds-mirna-mrna)
561 for the research community. This novel, rich resource enabled us to gain a network view of miR-
562 mediated gene regulation during human physiological and pathological wound repair in vivo. With the
563 same sequencing datasets, we have also analyzed circular RNA expression and their potential
564 interaction with miRs and miR targets(Toma et al., 2021), which results can be queried at
565 https://www.xulandenlab.com/humanwounds-circrna. These efforts result in many testable hypotheses
566 for future studies elucidating gene expression regulatory mechanisms underpinning tissue repair.

567 A limitation of our study is the lack of cell type specific miR expression data. Certain gene expression
568 changes detected in the tissue biopsies might be due to the changes of cellular compositions. To rule
569 out this possibility, we validated miR-mediated gene regulation in individual skin cell types (i.e.,
570 keratinocytes and fibroblasts) for several miRs surfaced in our analysis. However, to systemically
571 differentiate the gene expression regulation occurring in an individual cell from the altered cellular
572 composition in wound tissues requires future studies using single-cell small RNA sequencing, which
573 technology still remains challenging to be used at a scale for analyzing complex dynamics of tissue,
574 such as human skin and wounds, as it needs extensive cell handing and therefore has only been applied
575 to few cells(Nielsen & Pedersen, 2020). As new technologies for higher cellular resolution miRNA
576 analyses emerge, we hope that such approach will be feasible in a near future.

577

578 **Conclusion**

579 In conclusion, this genome-wide, integrative analysis of miR and mRNA expression in human skin and
580 wound tissues reinforce and extend the evidence about the functional role of miRs in wound repair and
581 their therapeutic potential for chronic wound treatment. By combining miR expression patterns with their
582 specific target gene expression context, we identified miRs highly relevant to VU pathology. This
583 rigorous and in-depth molecular characterization of human wound tissues adds a novel dimension to
584 our current knowledge mostly relying on non-human models and would serve as a unique platform and
585 valuable resource for further mechanistic studies of miRs with a high translational potential.

586 **Data availability**

587 Raw data of small RNA sequencing and long RNA sequencing performed in this study have been
588 deposited to NCBI's Gene Expression Omnibus (GEO) database under the accession number
589 GSE174661 (Reviewer access with a token 'cvmpqccylxgnzgj'). The microarray data are available from
590 the corresponding author upon reasonable request. In addition, the analyzed dataset is presented with
591 an online R Shiny app and can be accessed through a browsable web portal
592 (https://www.xulandenlab.com/humanwounds-mirna-mrna). The analysis source code is available at
593 https://github.com/Zhuang-Bio/miRNAprofiling.

594

595 **Competing Interest Statement**

596 The authors declare no conflict of interest.

597

598 **Funding and Acknowledgements**

599 We express our gratitude to the patients and healthy donors participating in this study. We thank Mona
600 Ståhle, Desiree Wiegleb Edström, Peter Berg, Fredrik Correa, Martin Gumulka, Mahsa Tayefi for clinical
601 sample collection; Helena Griehsel for technical support. We thank the Microarray core facility at Novum,
602 BEA, which is supported by the board of research at KI and the research committee at the Karolinska
603 hospital. The computations/data handling was enabled by resources in the projects sens2020010 and
604 2021/22-701 provided by the Swedish National Infrastructure for Computing (SNIC) at UPPMAX,
605 partially funded by the Swedish Research Council through grant agreement no. 2018-05973. This work
606 was supported by Swedish Research Council (Vetenskapsradet, 2016-02051 and 2020-01400), Ragnar
607 Söderbergs Foundation (M31/15), Welander and Finsens Foundation (Hudfonden), LEO foundation,
608 Ming Wai Lau Centre for Reparative Medicine, Karolinska Institutet, and R01AR073614 from
609 NIH/NIAMS (to MTC).

610

611 **Author Contributions**

612 N.X.L. and P.S. conceived and designed the study. P.S. collected most clinical samples with the
613 assistance of M.A.T.. L.Z., D.L., M.A.T., and X.B. performed the experiments. Z.L. and L.Z. carried out
614 bioinformatics analysis. I.P. and M.T.C contributed to data analyses and interpretation. Z.L., L.Z., and
615 N.X.L. wrote the manuscript, which was commented on by all authors.

616 **References**

617 Agarwal, V., Bell, G. W., Nam, J. W., & Bartel, D. P. (2015, Aug 12). Predicting effective microRNA target
618 sites in mammalian mRNAs. *Elife, 4*. https://doi.org/10.7554/eLife.05005

619
620 Blumberg, S. N., Maggi, J., Melamed, J., Golinko, M., Ross, F., & Chen, W. (2012, Dec). A histopathologic
621 basis for surgical debridement to promote healing of venous ulcers. *J Am Coll Surg, 215*(6), 751-757.
622 https://doi.org/10.1016/j.jamcollsurg.2012.08.008

623
624 Bolger, A. M., Lohse, M., & Usadel, B. (2014, Aug 1). Trimmomatic: a flexible trimmer for Illumina sequence
625 data. *Bioinformatics, 30*(15), 2114-2120. https://doi.org/10.1093/bioinformatics/btu170

626
627 Botchkarev, V. A. (2003, 2003/01/01/). Bone Morphogenetic Proteins and Their Antagonists in Skin and Hair
628 Follicle Biology. *Journal of Investigative Dermatology, 120*(1), 36-47.
629 https://doi.org/https://doi.org/10.1046/j.1523-1747.2003.12002.x

630
631 Cherone, J. M., Jorgji, V., & Burge, C. B. (2019). Cotargeting among microRNAs in the brain. *Genome*
632 *research, 29*(11), 1791-1804. https://doi.org/10.1101/gr.249201.119

633
634 Darwin, E., & Tomic-Canic, M. (2018, Dec). Healing Chronic Wounds: Current Challenges and Potential
635 Solutions. *Curr Dermatol Rep, 7*(4), 296-302. https://doi.org/10.1007/s13671-018-0239-4

636
637 Dobin, A., Davis, C. A., Schlesinger, F., Drenkow, J., Zaleski, C., Jha, S., Batut, P., Chaisson, M., & Gingeras,
638 T. R. (2013, Jan 1). STAR: ultrafast universal RNA-seq aligner. *Bioinformatics, 29*(1), 15-21.
639 https://doi.org/10.1093/bioinformatics/bts635

640
641 Elliot, S., Wikramanayake, T. C., Jozic, I., & Tomic-Canic, M. (2018, Apr). A Modeling Conundrum: Murine
642 Models for Cutaneous Wound Healing. *J Invest Dermatol, 138*(4), 736-740.
643 https://doi.org/10.1016/j.jid.2017.12.001

644
645 Eming, S. A., Martin, P., & Tomic-Canic, M. (2014, Dec 3). Wound repair and regeneration: mechanisms,
646 signaling, and translation. *Sci Transl Med, 6*(265), 265sr266.
647 https://doi.org/10.1126/scitranslmed.3009337

648
649 Erhard, F., Haas, J., Lieber, D., Malterer, G., Jaskiewicz, L., Zavolan, M., Dölken, L., & Zimmer, R. (2014).
650 Widespread context dependency of microRNA-mediated regulation. *Genome research, 24*(6), 906-919.
651 https://doi.org/10.1101/gr.166702.113

652
653 Ertosun, M. G., Hapil, F. Z., & Osman Nidai, O. (2016, 2016/10/01/). E2F1 transcription factor and its impact
654 on growth factor and cytokine signaling. *Cytokine & Growth Factor Reviews, 31*, 17-25.
655 https://doi.org/https://doi.org/10.1016/j.cytogfr.2016.02.001

656
657 Friedlander, M. R., Mackowiak, S. D., Li, N., Chen, W., & Rajewsky, N. (2012, Jan). miRDeep2 accurately
658 identifies known and hundreds of novel microRNA genes in seven animal clades. *Nucleic Acids Res,*
659 *40*(1), 37-52. https://doi.org/10.1093/nar/gkr688

660
661 Gu, Z., Eils, R., & Schlesner, M. (2016, Sep 15). Complex heatmaps reveal patterns and correlations in
662 multidimensional genomic data. *Bioinformatics, 32*(18), 2847-2849.
663 https://doi.org/10.1093/bioinformatics/btw313

Gu, Z., Gu, L., Eils, R., Schlesner, M., & Brors, B. (2014, Oct). circlize Implements and enhances circular visualization in R. *Bioinformatics, 30*(19), 2811-2812. https://doi.org/10.1093/bioinformatics/btu393

Guo, F., Carter, D. E., & Leask, A. (2014, Apr). miR-218 regulates focal adhesion kinase-dependent TGFβ signaling in fibroblasts. *Mol Biol Cell, 25*(7), 1151-1158. https://doi.org/10.1091/mbc.E13-08-0451

Guo, J., Zhang, J. F., Wang, W. M., Cheung, F. W., Lu, Y. F., Ng, C. F., Kung, H. F., & Liu, W. K. (2014). MicroRNA-218 inhibits melanogenesis by directly suppressing microphthalmia-associated transcription factor expression. *RNA Biol, 11*(6), 732-741. https://doi.org/10.4161/rna.28865

Hadley, W. (2016). ggplot2: Elegant Graphics for Data Analysis. *Springer-Verlag New York*. https://ggplot2.tidyverse.org

Han, H., Cho, J. W., Lee, S., Yun, A., Kim, H., Bae, D., Yang, S., Kim, C. Y., Lee, M., Kim, E., Lee, S., Kang, B., Jeong, D., Kim, Y., Jeon, H. N., Jung, H., Nam, S., Chung, M., Kim, J. H., & Lee, I. (2018, Jan 4). TRRUST v2: an expanded reference database of human and mouse transcriptional regulatory interactions. *Nucleic Acids Res, 46*(D1), D380-d386. https://doi.org/10.1093/nar/gkx1013

Herter, E. K., & Xu Landen, N. (2017, Mar 1). Non-Coding RNAs: New Players in Skin Wound Healing. *Adv Wound Care (New Rochelle), 6*(3), 93-107. https://doi.org/10.1089/wound.2016.0711

Hoversten, K. P., Kiemele, L. J., Stolp, A. M., Takahashi, P. Y., & Verdoorn, B. P. (2020, Sep). Prevention, Diagnosis, and Management of Chronic Wounds in Older Adults. *Mayo Clin Proc, 95*(9), 2021-2034. https://doi.org/10.1016/j.mayocp.2019.10.014

Ichihara, A., Jinnin, M., Yamane, K., Fujisawa, A., Sakai, K., Masuguchi, S., Fukushima, S., Maruo, K., & Ihn, H. (2011, Nov). microRNA-mediated keratinocyte hyperproliferation in psoriasis vulgaris. *Br J Dermatol, 165*(5), 1003-1010. https://doi.org/10.1111/j.1365-2133.2011.10497.x

Kaufman, C. K., Zhou, P., Pasolli, H. A., Rendl, M., Bolotin, D., Lim, K. C., Dai, X., Alegre, M. L., & Fuchs, E. (2003, Sep 1). GATA-3: an unexpected regulator of cell lineage determination in skin. *Genes Dev, 17*(17), 2108-2122. https://doi.org/10.1101/gad.1115203

Korotkevich, G., Sukhov, V., Budin, N., Shpak, B., Artyomov, M. N., & Sergushichev, A. (2021). Fast gene set enrichment analysis. *bioRxiv*, 060012. https://doi.org/10.1101/060012

Kozomara, A., Birgaoanu, M., & Griffiths-Jones, S. (2018). miRBase: from microRNA sequences to function. *Nucleic Acids Research, 47*(D1), D155-D162. https://doi.org/10.1093/nar/gky1141

Kurek, D., Garinis, G. A., van Doorninck, J. H., van der Wees, J., & Grosveld, F. G. (2007, Jan). Transcriptome and phenotypic analysis reveals Gata3-dependent signalling pathways in murine hair follicles. *Development, 134*(2), 261-272. https://doi.org/10.1242/dev.02721

Lai, X., Eberhardt, M., Schmitz, U., & Vera, J. (2019). Systems biology-based investigation of cooperating microRNAs as monotherapy or adjuvant therapy in cancer. *Nucleic Acids Research, 47*(15), 7753-7766. https://doi.org/10.1093/nar/gkz638

713
714 Landen, N. X., Li, D., & Stahle, M. (2016, Oct). Transition from inflammation to proliferation: a critical step
715 during wound healing. *Cell Mol Life Sci, 73*(20), 3861-3885. https://doi.org/10.1007/s00018-016-2268-
716 0

717
718 Langfelder, P., & Horvath, S. (2008, Dec 29). WGCNA: an R package for weighted correlation network
719 analysis. *BMC Bioinformatics, 9*, 559. https://doi.org/10.1186/1471-2105-9-559

720
721 Langfelder, P., Luo, R., Oldham, M. C., & Horvath, S. (2011, Jan 20). Is my network module preserved and
722 reproducible? *PLoS Comput Biol, 7*(1), e1001057. https://doi.org/10.1371/journal.pcbi.1001057

723
724 Langmead, B., Trapnell, C., Pop, M., & Salzberg, S. L. (2009, 2009/03/04). Ultrafast and memory-efficient
725 alignment of short DNA sequences to the human genome. *Genome Biology, 10*(3), R25.
726 https://doi.org/10.1186/gb-2009-10-3-r25

727
728 Lewis, B. P., Burge, C. B., & Bartel, D. P. (2005, 2005/01/14/). Conserved Seed Pairing, Often Flanked by
729 Adenosines, Indicates that Thousands of Human Genes are MicroRNA Targets. *Cell, 120*(1), 15-20.
730 https://doi.org/https://doi.org/10.1016/j.cell.2004.12.035

731
732 Lewis, C. J., Mardaryev, A. N., Poterlowicz, K., Sharova, T. Y., Aziz, A., Sharpe, D. T., Botchkareva, N. V., &
733 Sharov, A. A. (2014, Mar). Bone morphogenetic protein signaling suppresses wound-induced skin
734 repair by inhibiting keratinocyte proliferation and migration. *J Invest Dermatol, 134*(3), 827-837.
735 https://doi.org/10.1038/jid.2013.419

736
737 Li, D., Wang, A., Liu, X., Meisgen, F., Grunler, J., Botusan, I. R., Narayanan, S., Erikci, E., Li, X., Blomqvist,
738 L., Du, L., Pivarcsi, A., Sonkoly, E., Chowdhury, K., Catrina, S. B., Stahle, M., & Landen, N. X.
739 (2015, Aug 3). MicroRNA-132 enhances transition from inflammation to proliferation during wound
740 healing. *J Clin Invest, 125*(8), 3008-3026. https://doi.org/10.1172/JCI79052

741
742 Liang, L., Stone, R. C., Stojadinovic, O., Ramirez, H., Pastar, I., Maione, A. G., Smith, A., Yanez, V., Veves,
743 A., Kirsner, R. S., Garlick, J. A., & Tomic-Canic, M. (2016, Nov). Integrative analysis of miRNA and
744 mRNA paired expression profiling of primary fibroblast derived from diabetic foot ulcers reveals
745 multiple impaired cellular functions. *Wound Repair Regen, 24*(6), 943-953.
746 https://doi.org/10.1111/wrr.12470

747
748 Liang, P., Lv, C., Jiang, B., Long, X., Zhang, P., Zhang, M., Xie, T., & Huang, X. (2012, 2012/06/01/).
749 MicroRNA profiling in denatured dermis of deep burn patients. *Burns, 38*(4), 534-540.
750 https://doi.org/https://doi.org/10.1016/j.burns.2011.10.014

751
752 Liao, Y., Smyth, G. K., & Shi, W. (2013). featureCounts: an efficient general purpose program for assigning
753 sequence reads to genomic features. *Bioinformatics, 30*(7), 923-930.
754 https://doi.org/10.1093/bioinformatics/btt656

755
756 Liao, Y., Wang, J., Jaehnig, E. J., Shi, Z., & Zhang, B. (2019). WebGestalt 2019: gene set analysis toolkit with
757 revamped UIs and APIs. *Nucleic Acids Research, 47*(W1), W199-W205.
758 https://doi.org/10.1093/nar/gkz401

759
760 Liu, T., Zhang, L., Joo, D., & Sun, S.-C. (2017, 2017/07/14). NF-κB signaling in inflammation. *Signal*
761 *Transduction and Targeted Therapy, 2*(1), 17023. https://doi.org/10.1038/sigtrans.2017.23

762

763 Love, M. I., Huber, W., & Anders, S. (2014, 2014/12/05). Moderated estimation of fold change and dispersion
764 for RNA-seq data with DESeq2. *Genome Biology, 15*(12), 550. https://doi.org/10.1186/s13059-014-
765 0550-8

766
767 Luan, A., Hu, M. S., Leavitt, T., Brett, E. A., Wang, K. C., Longaker, M. T., & Wan, D. C. (2018, Jan 1).
768 Noncoding RNAs in Wound Healing: A New and Vast Frontier. *Adv Wound Care (New Rochelle),*
769 *7*(1), 19-27. https://doi.org/10.1089/wound.2017.0765

770
771 Mackowiak, S. D. (2011, Dec). Identification of novel and known miRNAs in deep-sequencing data with
772 miRDeep2. *Curr Protoc Bioinformatics, Chapter 12*, Unit 12 10.
773 https://doi.org/10.1002/0471250953.bi1210s36

774
775 Meng, Z., Zhou, D., Gao, Y., Zeng, M., & Wang, W. (2018, Apr). miRNA delivery for skin wound healing. *Adv*
776 *Drug Deliv Rev, 129*, 308-318. https://doi.org/10.1016/j.addr.2017.12.011

777
778 Nakashima, T., Jinnin, M., Etoh, T., Fukushima, S., Masuguchi, S., Maruo, K., Inoue, Y., Ishihara, T., & Ihn, H.
779 (2010, Dec 14). Down-regulation of mir-424 contributes to the abnormal angiogenesis via MEK1 and
780 cyclin E1 in senile hemangioma: its implications to therapy. *PLoS One, 5*(12), e14334.
781 https://doi.org/10.1371/journal.pone.0014334

782
783 Nie, X., Zhao, J., Ling, H., Deng, Y., Li, X., & He, Y. (2020, Sep). Exploring microRNAs in diabetic chronic
784 cutaneous ulcers: Regulatory mechanisms and therapeutic potential. *Br J Pharmacol, 177*(18), 4077-
785 4095. https://doi.org/10.1111/bph.15139

786
787 Nielsen, M. M., & Pedersen, J. S. (2020). miRNA activity inferred from single cell mRNA expression. *bioRxiv*,
788 2020.2007.2014.202051. https://doi.org/10.1101/2020.07.14.202051

789
790 Pachera, E., Assassi, S., Salazar, G. A., Stellato, M., Renoux, F., Wunderlin, A., Blyszczuk, P., Lafyatis, R.,
791 Kurreeman, F., de Vries-Bouwstra, J., Messemaker, T., Feghali-Bostwick, C. A., Rogler, G., van
792 Haaften, W. T., Dijkstra, G., Oakley, F., Calcagni, M., Schniering, J., Maurer, B., Distler, J. H., Kania,
793 G., Frank-Bertoncelj, M., & Distler, O. (2020, Sep 1). Long noncoding RNA H19X is a key mediator
794 of TGF-beta-driven fibrosis. *J Clin Invest, 130*(9), 4888-4905. https://doi.org/10.1172/JCI135439

795
796 Pappas, P. J., You, R., Rameshwar, P., Gorti, R., DeFouw, D. O., Phillips, C. K., Padberg, F. T., Jr., Silva, M.
797 B., Jr., Simonian, G. T., Hobson, R. W., 2nd, & Duran, W. N. (1999, Dec). Dermal tissue fibrosis in
798 patients with chronic venous insufficiency is associated with increased transforming growth factor-
799 beta1 gene expression and protein production. *J Vasc Surg, 30*(6), 1129-1145.
800 https://doi.org/10.1016/s0741-5214(99)70054-6

801
802 Pastar, I., Marjanovic, J., Stone, R. C., Chen, V., Burgess, J. L., Mervis, J. S., & Tomic-Canic, M. (2021, Mar
803 10). Epigenetic regulation of cellular functions in wound healing. *Exp Dermatol*.
804 https://doi.org/10.1111/exd.14325

805
806 Pastar, I., Wong, L. L., Egger, A. N., & Tomic-Canic, M. (2018, May). Descriptive vs mechanistic scientific
807 approach to study wound healing and its inhibition: Is there a value of translational research involving
808 human subjects? *Exp Dermatol, 27*(5), 551-562. https://doi.org/10.1111/exd.13663

809
810 Ramirez, H. A., Pastar, I., Jozic, I., Stojadinovic, O., Stone, R. C., Ojeh, N., Gil, J., Davis, S. C., Kirsner, R. S.,
811 & Tomic-Canic, M. (2018, May). Staphylococcus aureus Triggers Induction of miR-15B-5P to

Diminish DNA Repair and Deregulate Inflammatory Response in Diabetic Foot Ulcers. *J Invest Dermatol, 138*(5), 1187-1196. https://doi.org/10.1016/j.jid.2017.11.038

Reinke, J. M., & Sorg, H. (2012). Wound repair and regeneration. *Eur Surg Res, 49*(1), 35-43. https://doi.org/10.1159/000339613

Ritchie, M. E., Phipson, B., Wu, D., Hu, Y., Law, C. W., Shi, W., & Smyth, G. K. (2015). limma powers differential expression analyses for RNA-sequencing and microarray studies. *Nucleic Acids Research, 43*(7), e47-e47. https://doi.org/10.1093/nar/gkv007

Ru, Y., Kechris, K. J., Tabakoff, B., Hoffman, P., Radcliffe, R. A., Bowler, R., Mahaffey, S., Rossi, S., Calin, G. A., Bemis, L., & Theodorescu, D. (2014). The multiMiR R package and database: integration of microRNA–target interactions along with their disease and drug associations. *Nucleic Acids Research, 42*(17), e133-e133. https://doi.org/10.1093/nar/gku631

Rupaimoole, R., & Slack, F. J. (2017, Mar). MicroRNA therapeutics: towards a new era for the management of cancer and other diseases. *Nat Rev Drug Discov, 16*(3), 203-222. https://doi.org/10.1038/nrd.2016.246

Segre, J. A., Bauer, C., & Fuchs, E. (1999, 1999/08/01). Klf4 is a transcription factor required for establishing the barrier function of the skin. *Nature Genetics, 22*(4), 356-360. https://doi.org/10.1038/11926

Sen, C. K., & Roy, S. (2012, Dec). OxymiRs in cutaneous development, wound repair and regeneration. *Semin Cell Dev Biol, 23*(9), 971-980. https://doi.org/10.1016/j.semcdb.2012.09.012

Shannon, P., Markiel, A., Ozier, O., Baliga, N. S., Wang, J. T., Ramage, D., Amin, N., Schwikowski, B., & Ideker, T. (2003, Nov). Cytoscape: a software environment for integrated models of biomolecular interaction networks. *Genome Res, 13*(11), 2498-2504. https://doi.org/10.1101/gr.1239303

Shen, Z., Sun, J., Shao, J., & Xu, J. (2020). Ultraviolet B irradiation enhances the secretion of exosomes by human primary melanocytes and changes their exosomal miRNA profile. *PLoS One, 15*(8), e0237023. https://doi.org/10.1371/journal.pone.0237023

Stavast, C. J., & Erkeland, S. J. (2019). The Non-Canonical Aspects of MicroRNAs: Many Roads to Gene Regulation. *Cells, 8*(11), 1465. https://doi.org/10.3390/cells8111465

Stojadinovic, O., Pastar, I., Nusbaum, A. G., Vukelic, S., Krzyzanowska, A., & Tomic-Canic, M. (2014, Mar-Apr). Deregulation of epidermal stem cell niche contributes to pathogenesis of nonhealing venous ulcers. *Wound Repair Regen, 22*(2), 220-227. https://doi.org/10.1111/wrr.12142

Stojadinovic, O., Pastar, I., Vukelic, S., Mahoney, M. G., Brennan, D., Krzyzanowska, A., Golinko, M., Brem, H., & Tomic-Canic, M. (2008, Dec). Deregulation of keratinocyte differentiation and activation: a hallmark of venous ulcers. *J Cell Mol Med, 12*(6b), 2675-2690. https://doi.org/10.1111/j.1582-4934.2008.00321.x

Stone, R. C., Stojadinovic, O., Rosa, A. M., Ramirez, H. A., Badiavas, E., Blumenberg, M., & Tomic-Canic, M. (2017, Jan 4). A bioengineered living cell construct activates an acute wound healing response in venous leg ulcers. *Sci Transl Med, 9*(371). https://doi.org/10.1126/scitranslmed.aaf8611

Stone, R. C., Stojadinovic, O., Sawaya, A. P., Glinos, G. D., Lindley, L. E., Pastar, I., Badiavas, E., & Tomic-Canic, M. (2020, Mar). A bioengineered living cell construct activates metallothionein/zinc/MMP8 and inhibits TGFβ to stimulate remodeling of fibrotic venous leg ulcers. *Wound Repair Regen, 28*(2), 164-176. https://doi.org/10.1111/wrr.12778

Subramanian, A., Tamayo, P., Mootha, V. K., Mukherjee, S., Ebert, B. L., Gillette, M. A., Paulovich, A., Pomeroy, S. L., Golub, T. R., Lander, E. S., & Mesirov, J. P. (2005, Oct 25). Gene set enrichment analysis: a knowledge-based approach for interpreting genome-wide expression profiles. *Proc Natl Acad Sci U S A, 102*(43), 15545-15550. https://doi.org/10.1073/pnas.0506580102

[Record #219 is using a reference type undefined in this output style.]

Tong, Z., Cui, Q., Wang, J., & Zhou, Y. (2019, Jan 8). TransmiR v2.0: an updated transcription factor-microRNA regulation database. *Nucleic Acids Res, 47*(D1), D253-d258. https://doi.org/10.1093/nar/gky1023

Vivas, A., Lev-Tov, H., & Kirsner, R. S. (2016, Aug 2). Venous Leg Ulcers. *Ann Intern Med, 165*(3), Itc17-itc32. https://doi.org/10.7326/aitc201608020

Wu, J., Li, X., Li, D., Ren, X., Li, Y., Herter, E. K., Qian, M., Toma, M. A., Wintler, A. M., Serezal, I. G., Rollman, O., Stahle, M., Wikstrom, J. D., Ye, X., & Landen, N. X. (2020, Feb). MicroRNA-34 Family Enhances Wound Inflammation by Targeting LGR4. *J Invest Dermatol, 140*(2), 465-476 e411. https://doi.org/10.1016/j.jid.2019.07.694

Wu, Y. E., Parikshak, N. N., Belgard, T. G., & Geschwind, D. H. (2016, Nov). Genome-wide, integrative analysis implicates microRNA dysregulation in autism spectrum disorder. *Nat Neurosci, 19*(11), 1463-1476. https://doi.org/10.1038/nn.4373

Yang, L., Dai, J., Li, F., Cheng, H., Yan, D., & Ruan, Q. (2017, Sep 19). The expression and function of miR-424 in infantile skin hemangioma and its mechanism. *Sci Rep, 7*(1), 11846. https://doi.org/10.1038/s41598-017-10674-7

Zhang, B., & Horvath, S. (2005). A general framework for weighted gene co-expression network analysis. *Stat Appl Genet Mol Biol, 4*, Article17. https://doi.org/10.2202/1544-6115.1128

Zhao, B., Chen, Y., Yang, N., Chen, Q., Bao, Z., Liu, M., Hu, S., Li, J., & Wu, X. (2019, Nov). miR-218-5p regulates skin and hair follicle development through Wnt/β-catenin signaling pathway by targeting SFRP2. *J Cell Physiol, 234*(11), 20329-20341. https://doi.org/10.1002/jcp.28633

Zhou, L., Chen, J., Li, Z., Li, X., Hu, X., Huang, Y., Zhao, X., Liang, C., Wang, Y., Sun, L., Shi, M., Xu, X., Shen, F., Chen, M., Han, Z., Peng, Z., Zhai, Q., Chen, J., Zhang, Z., Yang, R., Ye, J., Guan, Z., Yang, H., Gui, Y., Wang, J., Cai, Z., & Zhang, X. (2010, Dec 30). Integrated profiling of microRNAs and mRNAs: microRNAs located on Xq27.3 associate with clear cell renal cell carcinoma. *PLoS One, 5*(12), e15224. https://doi.org/10.1371/journal.pone.0015224

907 **Figures with legends**

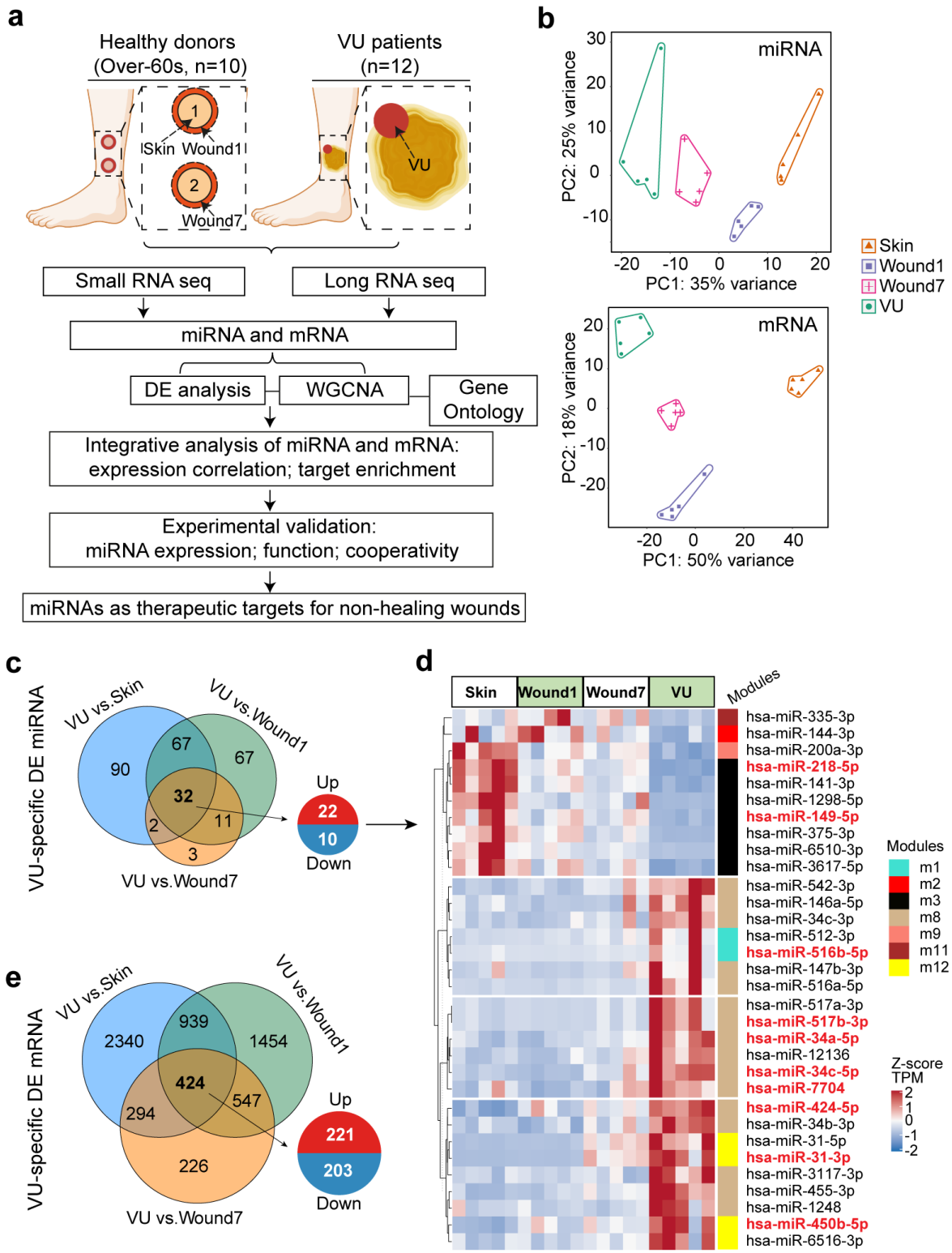

908

909 **Fig. 1** Paired profiling of miRNA and mRNA expression in human wounds. **a** Schematic of analysis in

910 this study. **b** PCA plots based on miRNA (upper panel) and mRNA (lower panel) expression profiles.

911 Each dot indicates an individual sample. The numbers of differentially expressed (DE) miRNAs **c** and

912 mRNAs **e** in VU (n=5) compared to the Skin, Wound1, and Wound7 from 5 healthy donors are shown
913 in Venn diagrams. FDR < 0.05, fold change ≥ 2 for miRNAs and ≥ 1.5 for mRNAs. **d** The heatmap
914 depicts the 32 miRNAs specifically dysregulated in the VU with scaled expression values (Z-scores).
915 WGCNA modules of each miRNA belongs to are marked with color bars. The miRNAs with
916 experimentally validated expression changes are highlighted in red.

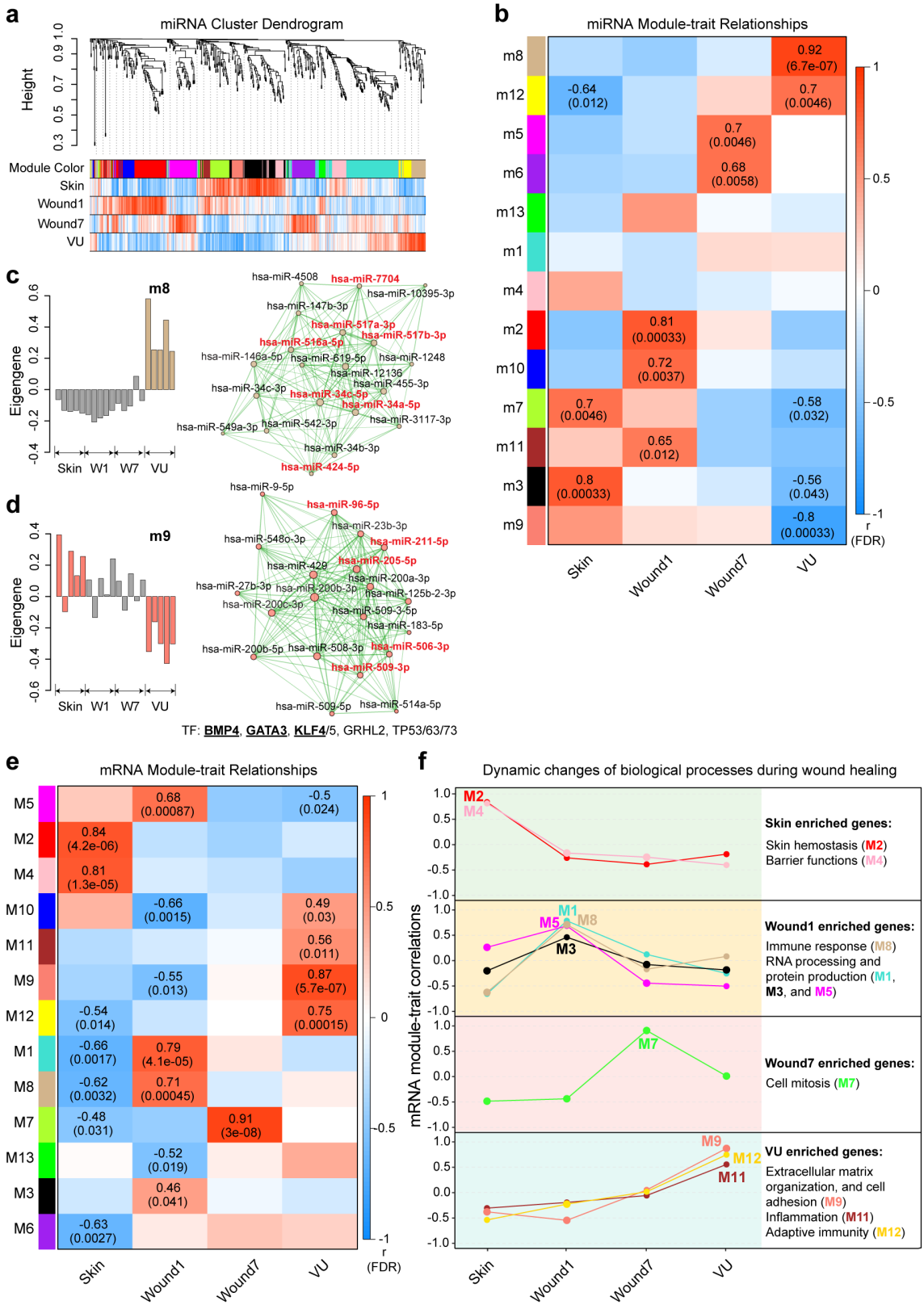

Fig. 2 Weighted gene co-expression network analysis (WGCNA) of miRNAs and mRNAs in wound healing. **a** Cluster dendrogram shows miRNA co-expression modules: each branch corresponds to a module, and each leaf indicates a single miRNA. Color bars below show the module assignment (the

921 1st row) and Pearson correlation coefficients between miRNA expression and the sample groups (the
922 2nd to the 5th row: red and blue lines represent positive and negative correlations, respectively). **b**
923 Heatmap shows Pearson correlations between miRNA module eigengenes (ME) and the sample
924 groups. The correlation coefficients and the adjusted *P-values* (FDR) are shown where the FDRs are
925 less than 0.05. For the VU-associated modules m8 **c** and m9 **d**, bar plots (left) depict the ME values
926 across the 20 samples analyzed by RNA-seq, and network plots (right) show the top 20 miRNAs with
927 the highest kME values in each module. Node size and edge thickness are proportional to the kME
928 values and the weighted correlations between two connected miRNAs, respectively. The miRs with their
929 targetome enriched with VU-mRNA signature (see Fig. 4b) are highlighted in red. Transcription factors
930 (TFs) with their targets enriched in the m9 module (Fisher's exact test: FDR < 0.05) are listed below the
931 network, and TFs differentially expressed in VU are underlined. **e** Heatmap shows Pearson correlations
932 between mRNA MEs and the sample groups. **f** The gene expression pattern of each module across all
933 the sample groups is depicted with line charts. Gene ontology analysis of biological processes enriched
934 in each module is shown at the right.

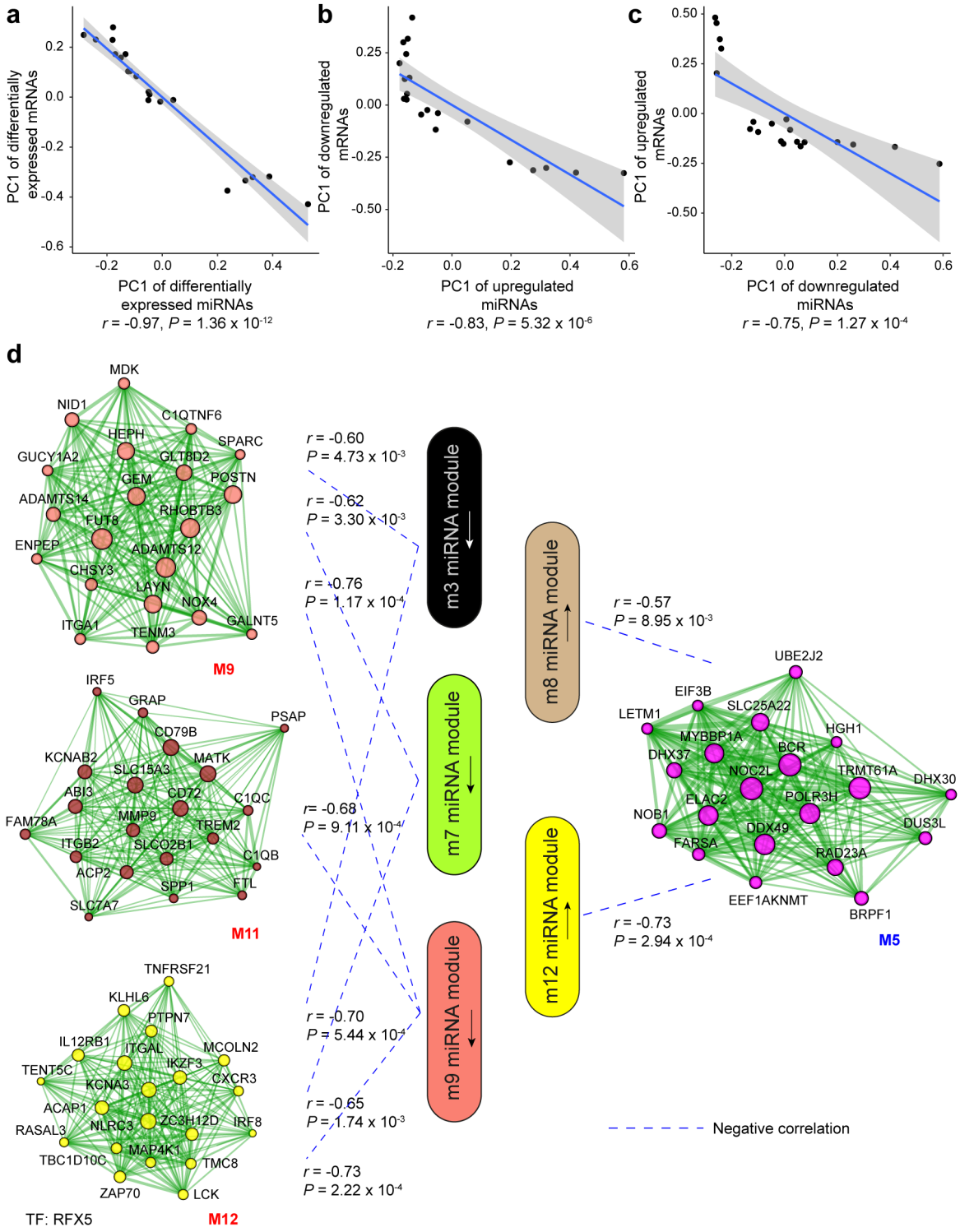

935

936 **Fig. 3** Correlation analysis between miRNA and mRNA expression changes in VU. **a-c** Correlations
937 between the first principal component (PC1) of VU-associated differentially expressed (DE) miRNAs,
938 and the PC1 of VU DE mRNAs predicted as miRNA targets. **d** PC1 correlations between the hub
939 miRNAs and their predicted targets in the VU-associated miRNA and mRNA modules. Pearson

940 correlation coefficients (*r*) and *P* values are shown. The mRNA networks are plotted with the top 20
941 most connected module genes. Transcription factors (TFs) with targets enriched in the VU-associated
942 modules are listed below the networks.

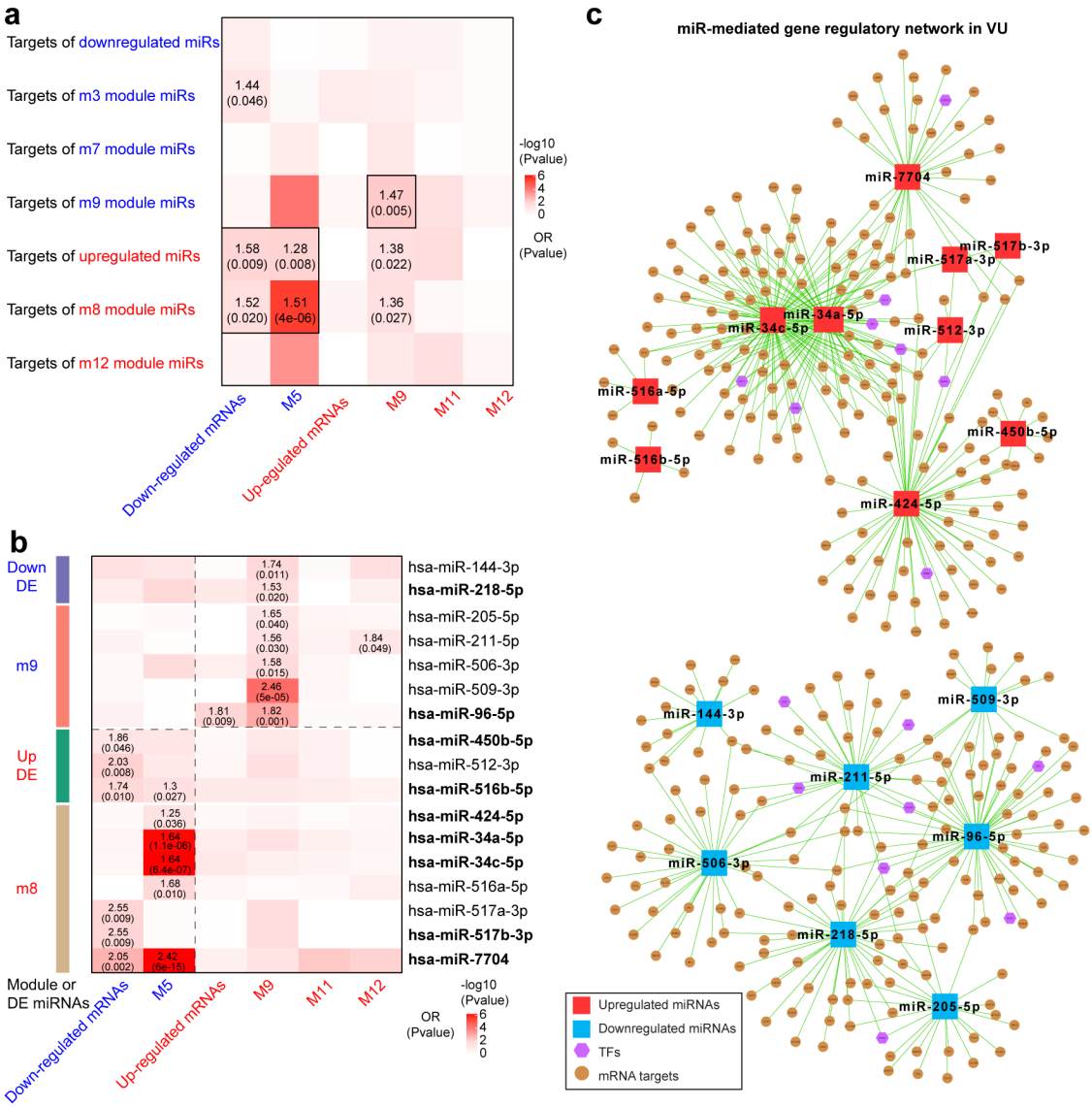

Fig. 4 Integrative analysis of miRNA and mRNA expression changes in VU. Heatmaps show the enrichment for VU-affected mRNAs and mRNA modules in the top targets of **a** VU-associated DE miRNAs and miR modules and **b** the individual candidate miRNAs. Odds ratio (OR) and *P* values are indicated when OR > 1 and *P-value* < 0.05 (Fisher's exact test). The miRNAs with experimentally validated expression changes are highlighted in bold. **c** miR-mediated gene regulatory networks in VU are constructed with the miRNAs in Fig. 4b, the mRNAs predicted as the strongest targets and with anti-correlated expression patterns (Pearson correlation, *P-value* < 0.05 and r < 0) with these miRNAs in human wounds, and the TFs regulating these miRNAs' expression from the TransmiR v2 database. An enlarged version of these networks can be found in Fig. S6 and S7.

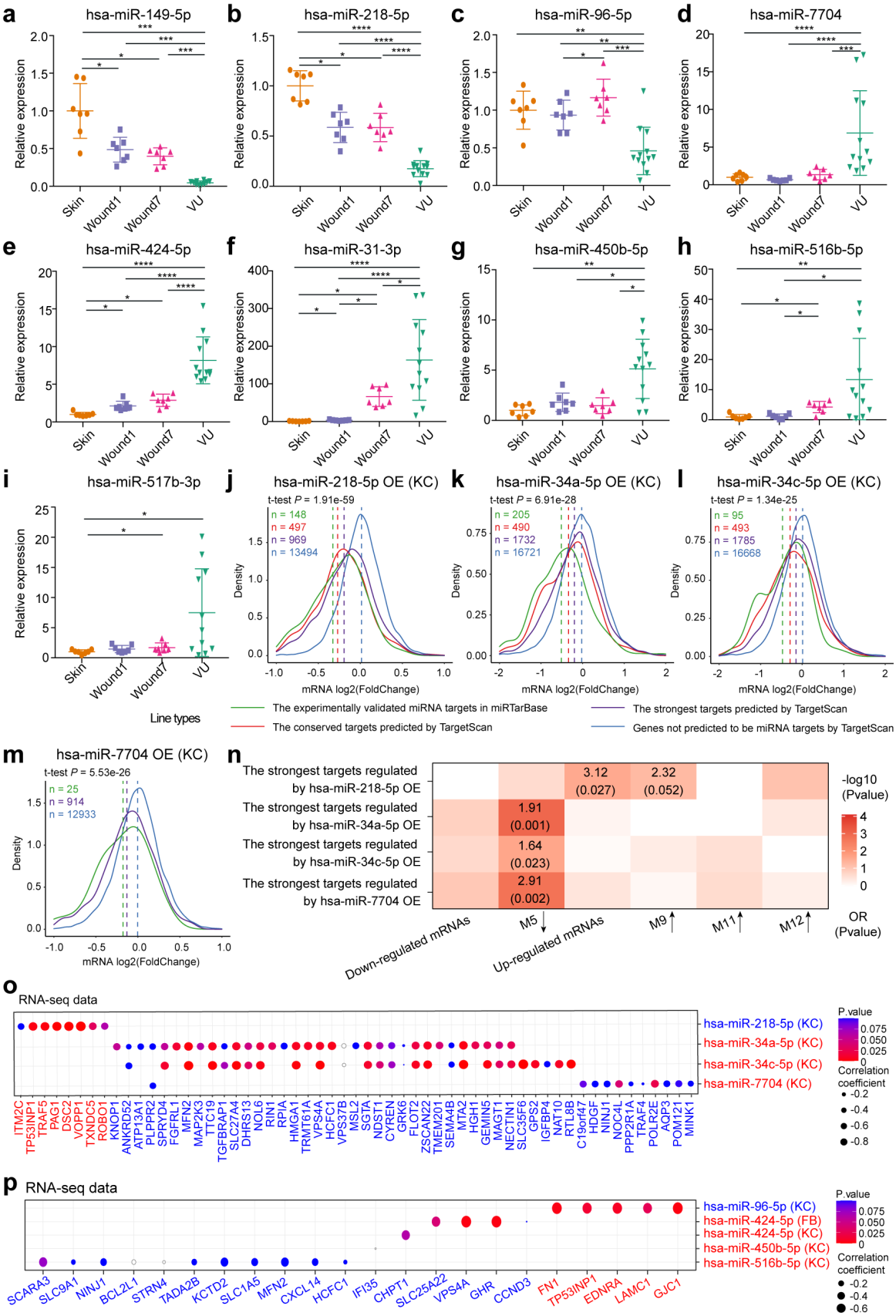

954

955 **Fig. 5** Experimental validation of miRNAs' expression and targets in human skin wounds. **a-i** qRT-PCR

956 analysis of VU-associated DE miRNAs in the skin, day 1 and day 7 acute wounds from 7 healthy donors
957 and venous ulcers (VU) from 12 patients. Wilcoxon signed-rank test was used for the comparison
958 between Skin, Wound1, and Wound7; Mann-Whitney U test was used for comparing VU with the skin
959 and acute wounds. *P < 0.05, **P < 0.01, ***P < 0.001, ****P < 0.0001. **j-m** Microarray analysis was
960 performed in keratinocytes (KC) with miR-218-5p (**J**), miR-34a-5p **k**, miR-34c-5p **l**, or miR-7704 **m**
961 overexpression (OE), and density plots of mRNAs $\log_2$(fold change) are shown. Wilcoxon t-tests were
962 performed to compare the TargetScan predicted strongest targets (purple) with the non-targets (blue)
963 for each of these miRNAs. The conserved and experimentally validated targets are marked with red
964 and green colors, respectively. Dotted lines depict the average log2(fold change) values for each mRNA
965 group. **n** A heatmap shows the enrichment for VU-affected mRNAs and mRNA modules in the targets
966 of miR-218-5p, miR-34a-5p, miR-34c-5p, or miR-7704 validated by the microarray analysis. Odds ratio
967 (OR) and P values are shown when OR > 1 and *P-value* < 0.05 (Fisher's exact test). **o, p** For each of
968 the miRNAs (miR-218-5p, miR-34a-5p, miR-34c-5p, miR-7704, miR-96, miR-424, miR-450b, and miR-
969 516b) and its targets validated by the microarray analysis of KC or fibroblasts (FB), Pearson correlation
970 analysis was performed between their expression values in human skin and wound samples shown by
971 RNA-seq. Grey circles indicate correlation coefficients > 0.

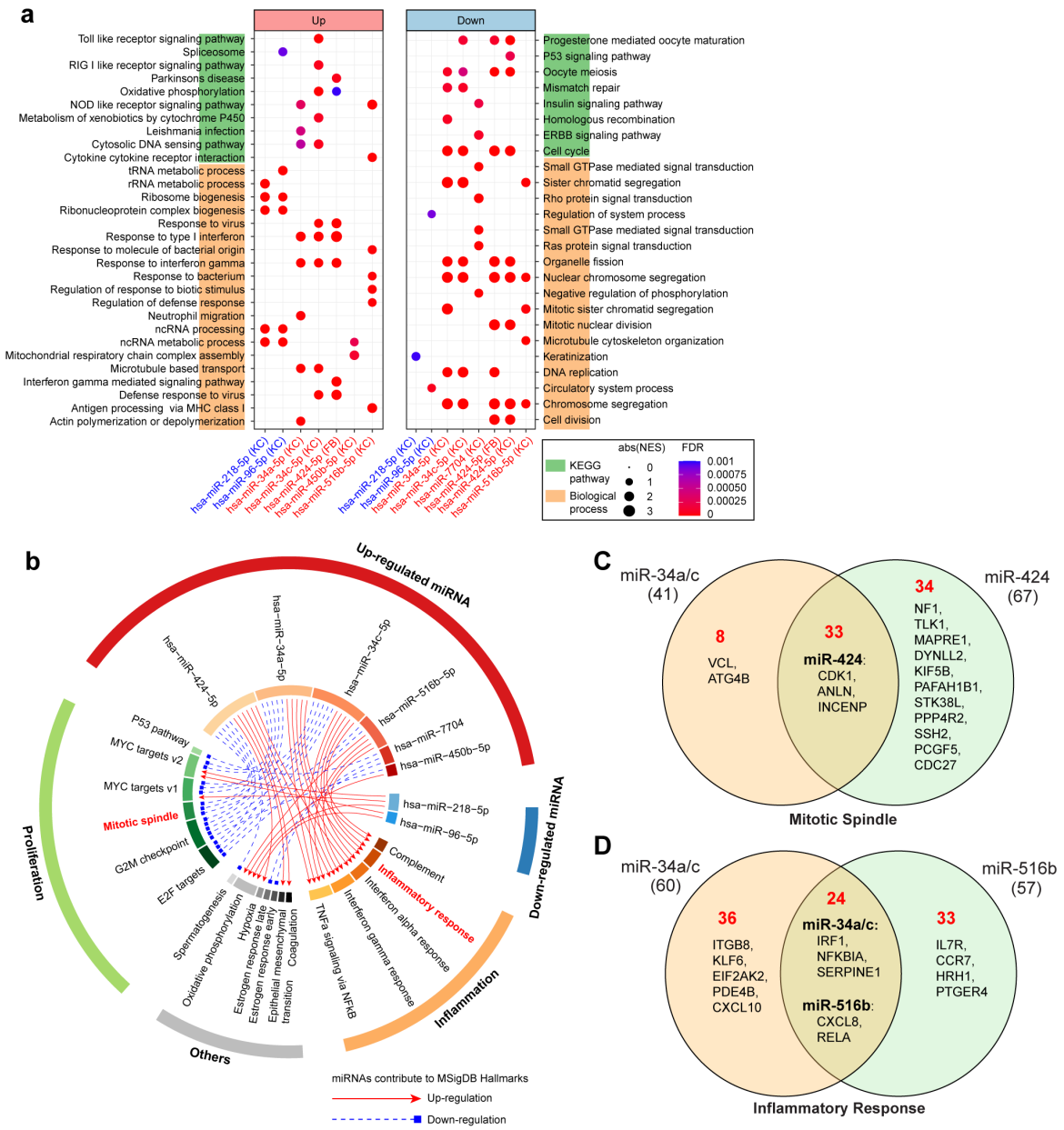

Fig. 6 Cooperativity of VU pathology-relevant miRNAs. For the microarray data in keratinocytes (KC) or fibroblasts (FB) with miR-218-5p, miR-96-5p, miR-34a-5p, miR-34c-5p, miR-7704, miR-424-5p, miR-516-5p overexpression, we analyzed KEGG pathways, biological processes **a**, and Molecular Signatures Database (MSigDB) hallmarks **b** enriched by the genes up-or down-regulated by these miRNAs. Venn diagrams show the numbers of the mitotic spindle-related genes regulated by miR-34a/c-5p and miR-424-5p **c** and the inflammatory response-related genes regulated by miR-34a/c-5p and miR-516b-5p **d** (fold change > 1.2, *P*-value < 0.05) in the microarray analysis of keratinocytes

980 overexpressing these miRNAs. Among the regulated genes, the targets of each miRNA are depicted in
981 the plots.

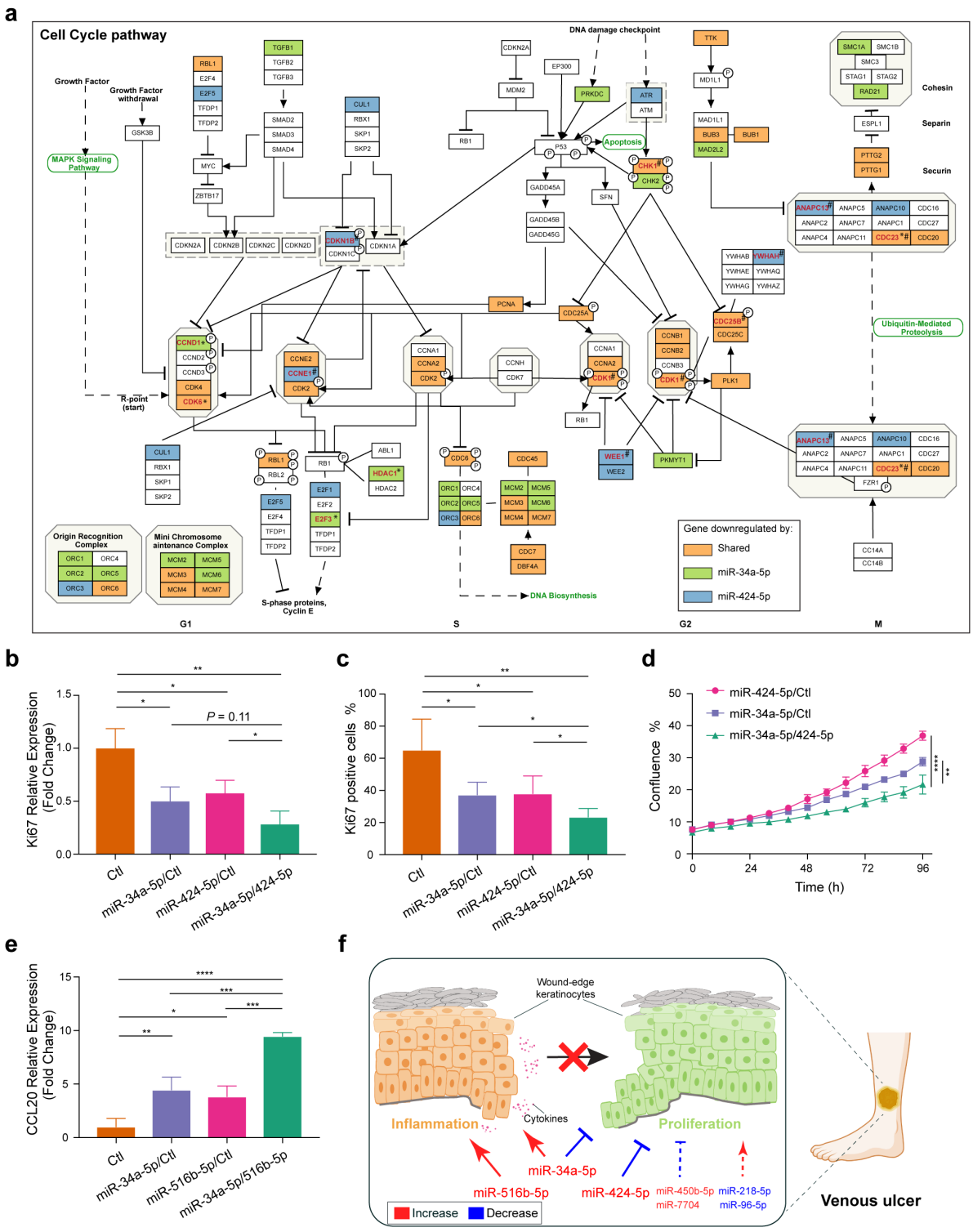

Fig. 7 Cooperation of miR-34a, miR-424, and miR-516 in regulating keratinocyte proliferation and inflammatory response. **a** In the KEGG cell cycle pathway map, genes regulated by miR-34a-5p or miR-424-5p or both miRNAs as shown in the microarray analysis of keratinocytes are marked with green, blue, and orange colors, respectively. Among the regulated genes, the miRNA targets are highlighted

987 in red and labeled with * for miR-34a targets, # for miR-424 targets, *# for the gene co-targeted by both
988 miRNAs. Ki67 expression was detected in keratinocytes transfected with miR-34a-5p or miR-424-5p
989 mimics alone or both mimics for 24 hours (n = 3) by qRT-PCR **b** and immunofluorescence staining (n
990 = 5 for Ctl and miR-34a-5p/424-5p, n = 4 for miR-34a-5p/ctl and miR-424-5p/ctl) **c**. **d** The growth of the
991 transfected keratinocytes (n = 3) was analyzed with a live cell imaging system. **e** qRT-PCR analysis of
992 CCL20 in keratinocytes transfected with miR-34a-5p or miR-516b-5p mimics alone or both mimics for
993 24 hours (n = 3). **f** Proposed mechanism by which VU-dysregulated miRNAs cooperatively contribute
994 to the stalled wound healing characterized with failed inflammation-proliferation transition. *$P < 0.05$;
995 **$P < 0.01$; ***$P < 0.001$ and ****$P<0.0001$ by unpaired two-tailed Student's t-test **b, c,** and **e** and Two-
996 way ANOVA **e**. Data are presented as mean ± SD.

997 **Supplements**

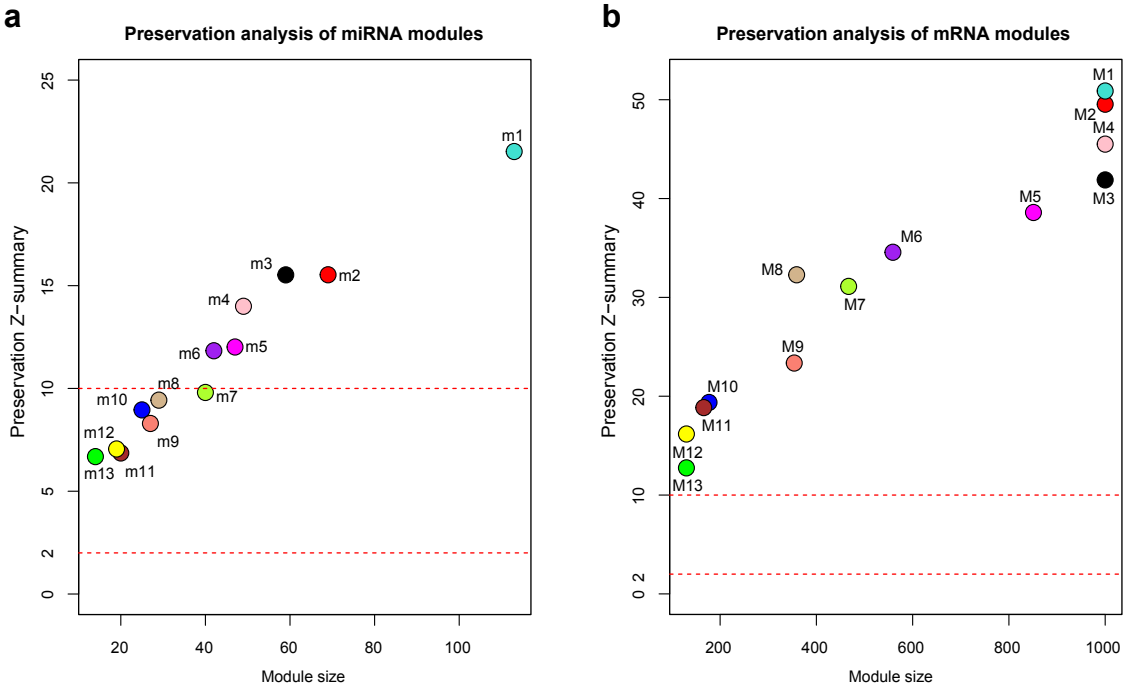

998

999 **Fig. S1 Preservation analysis of miRNA a and mRNA b co-expression modules.** The standardized
1000 Z-scores were calculated for each module by permutating 200 times using the 20 samples analyzed by
1001 RNA-seq as reference and test datasets. Modular preservation is strong if Z-summary > 10, weak to
1002 moderate if 2 < Z-summary < 10, no evidence of preservation if Z-summary ≤ 2. miRNA modules.

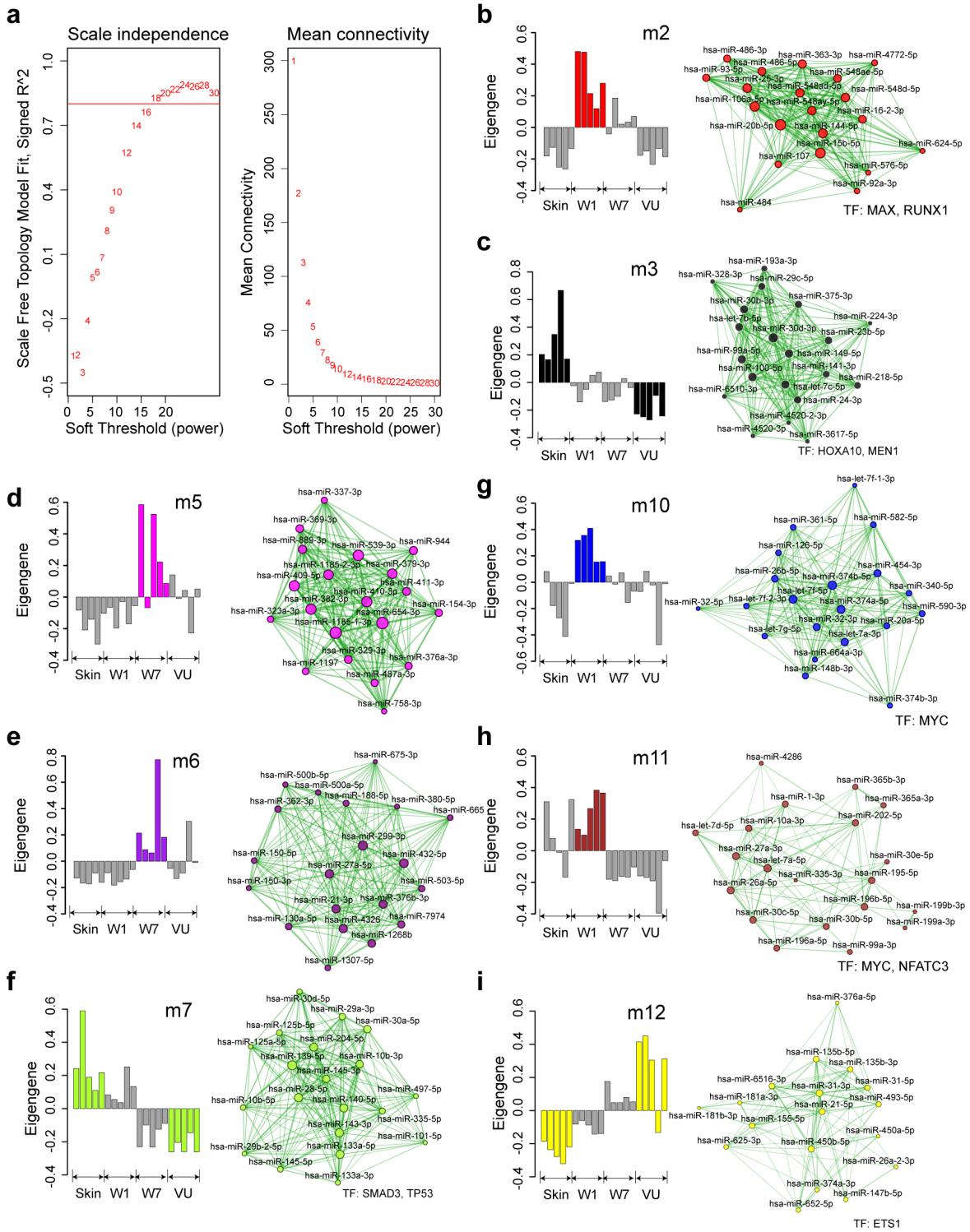

Fig. S2 Weighted gene co-expression network analysis (WGCNA) of miRNAs in human skin wound healing (related to Fig. 2a–d). **a** The scale-free topology fit index (left) and mean connectivity (right) for various soft-threshold powers. The red line indicates signed $R^2 = 0.8$. **b–i** Bar plots (left) depict the ME values across the 20 samples analyzed by RNA-seq and network plots (right) show the top 20 miRNAs with the highest kME values in each module. Node size and edge thickness are proportional

1009 to the kME values and the weighted correlations between two connected miRNAs, respectively.
1010 Transcription factors (TFs) with their targets enriched in the modules (Fisher's exact test: FDR < 0.05)
1011 are listed below the networks.

1012

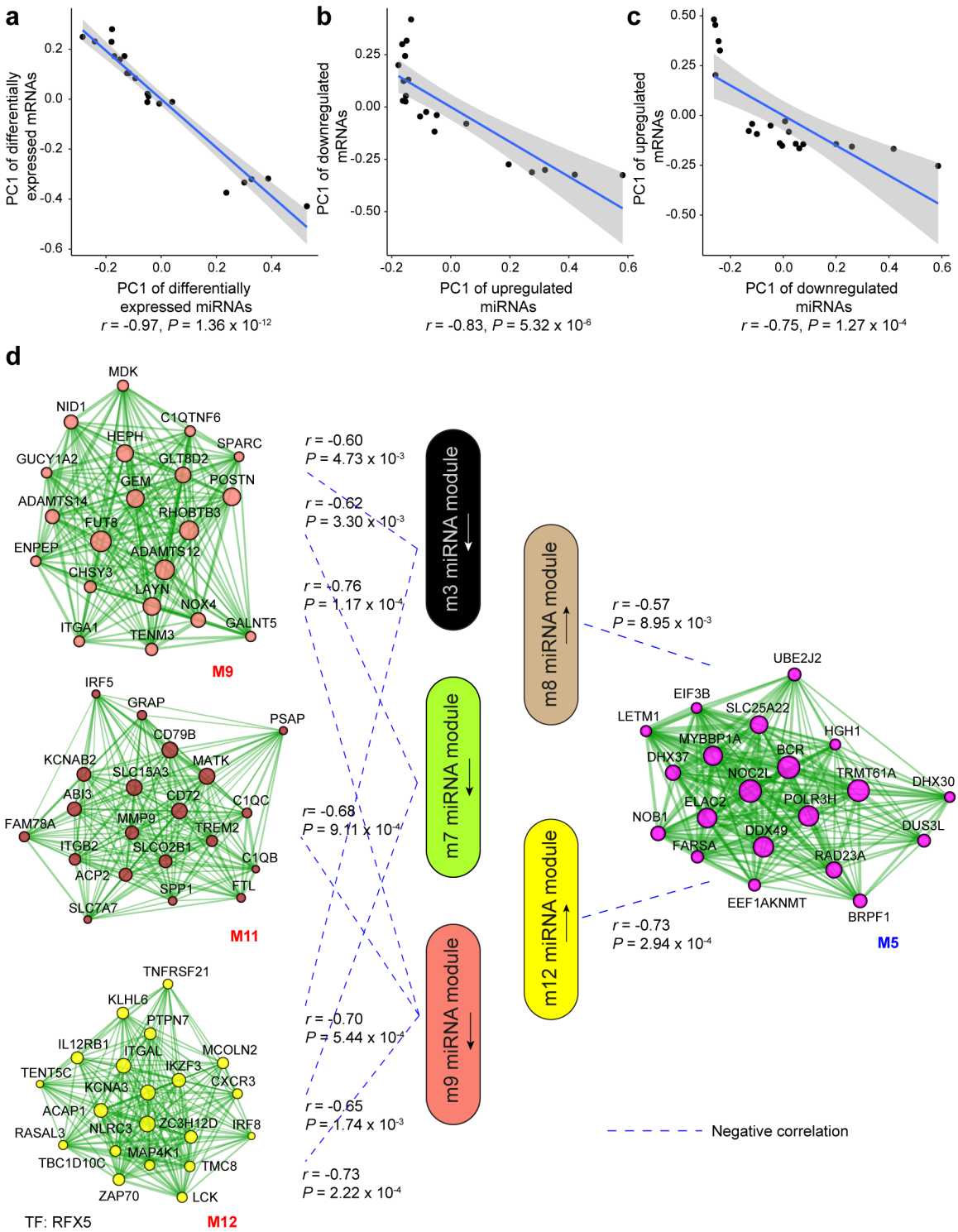

1013

1014 **Fig. S3 Transcription factors (TFs) with targets enriched in the miRNA m9 module. a** Pearson

1015 correlations between the first principal component (PC1) of miRNAs module m9 and the expression of

1016 BMP4, GATA3, or KLF4. **b** BMP4, GATA3, and KLF4 expression in the skin, day 1 and day 7 acute

1017 wounds from five healthy donors and in five venous ulcers analyzed by RNA-sequencing. Mann-
1018 Whitney t-test, $^{**}P < 0.01$.

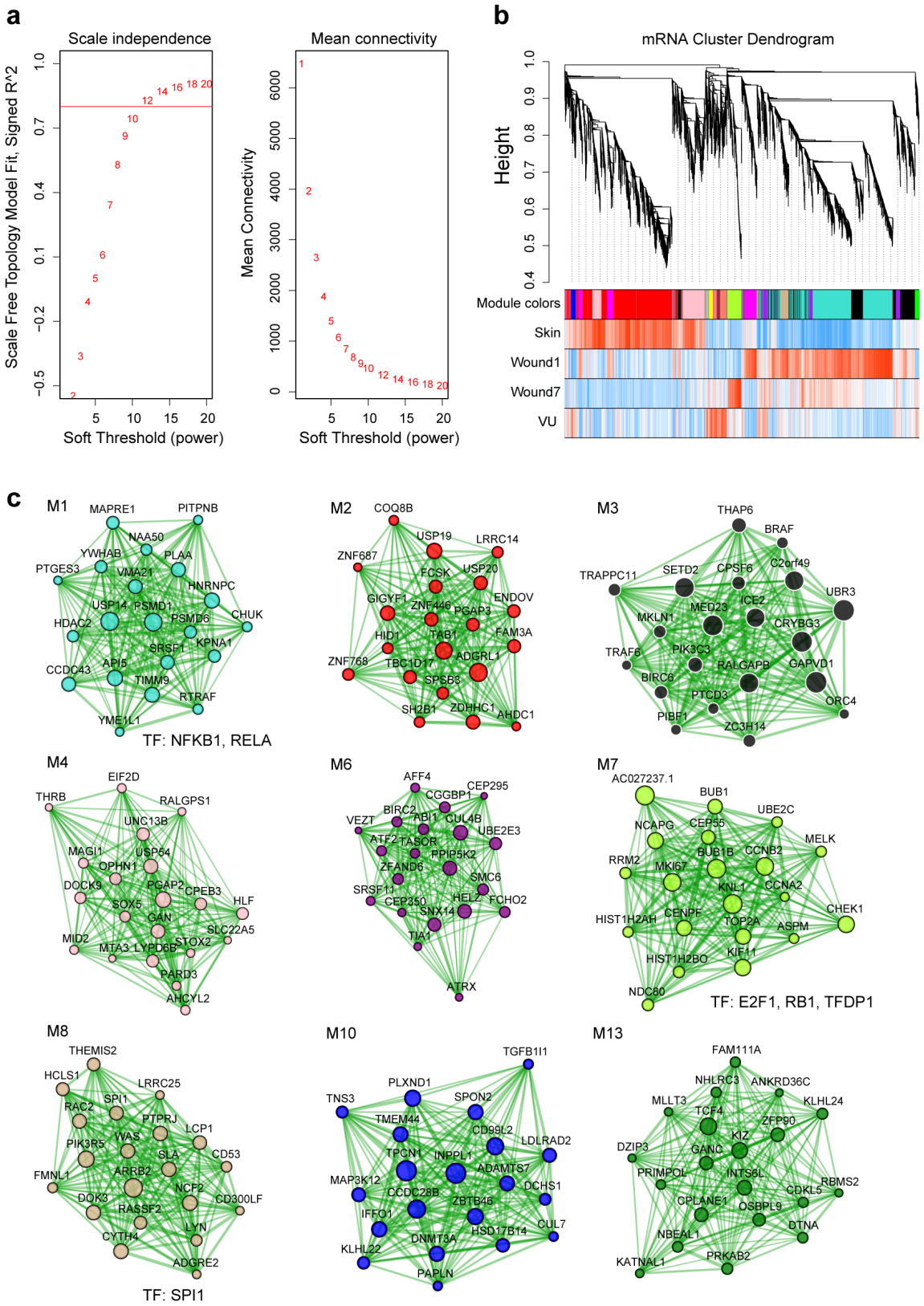

Fig. S4 Weighted gene co-expression network analysis (WGCNA) of mRNAs in human skin wound healing (related to Fig. 2e). **a** The scale-free topology fit index (left) and mean connectivity (right) for various soft-threshold powers. The red line indicates signed R^2 = 0.8. **b** Cluster dendrogram shows mRNA co-expression modules: each branch corresponds to a module, and each leaf indicates

1024 a single miRNA. Color bars below show the module assignment (the 1st row) and Pearson correlation
1025 coefficients between mRNA expression and the sample groups (the 2nd to the 5th row: red and blue lines
1026 represent positive and negative correlations, respectively). **c** Network plots of mRNA modules: the top
1027 20 mRNAs with the highest kME values in each module were plotted in the networks. Node size and
1028 edge thickness are proportional to the kME values and the weighted correlations between two
1029 connected mRNAs, respectively. Transcription factors (TFs) with their targets enriched in the modules
1030 (Fisher's exact test: FDR < 0.05) are listed below the networks.

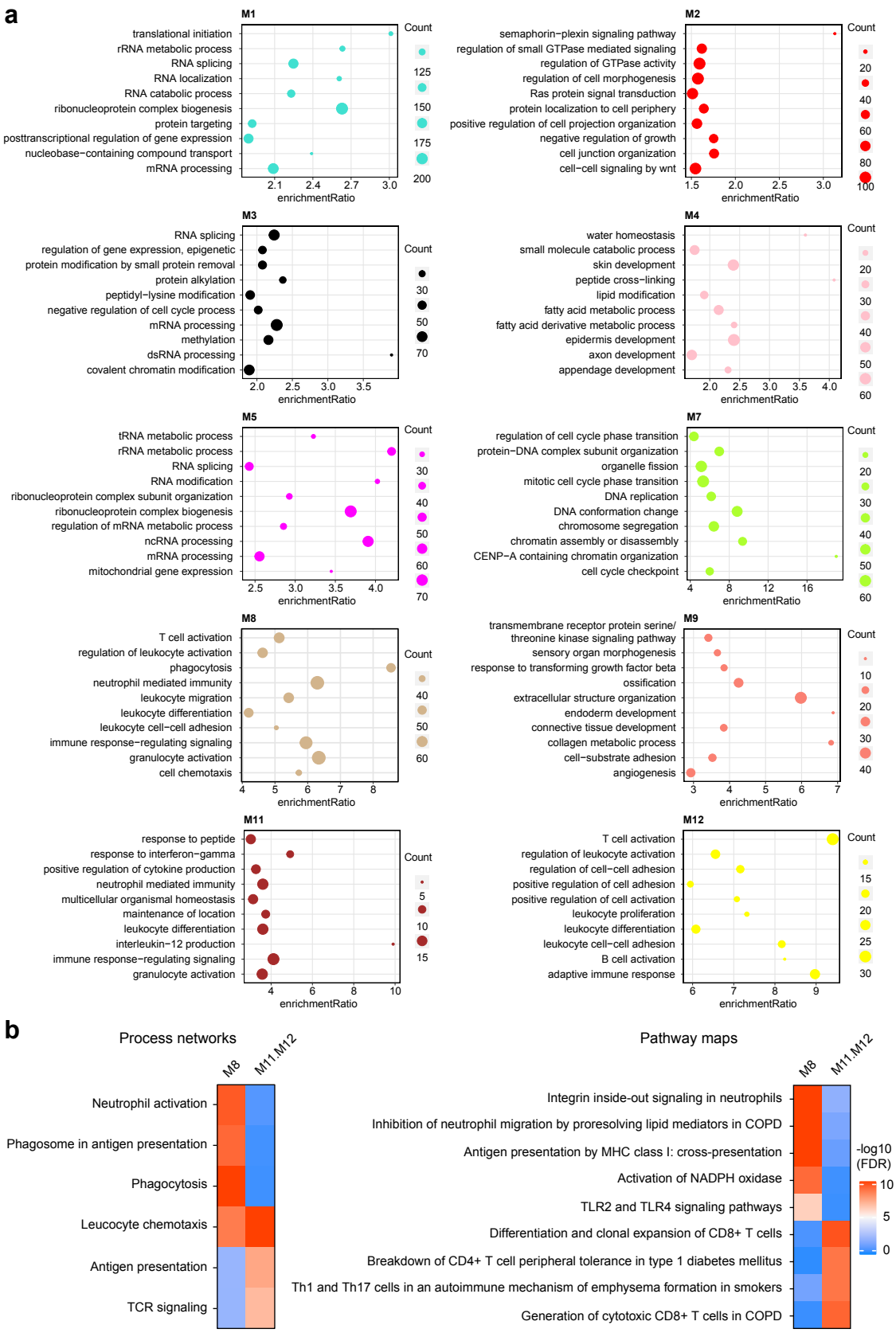

Fig. S5 Functional enrichment analysis for mRNA modules. a The top ten gene ontology (GO) terms with FDR less than 0.05 are shown for each module (related to Fig. 2f). **b** MetaCore analysis

1034 based on a curated database identified the process networks (left) and pathway maps (right) enriched

1035 in the M8 or the combined M11.M12 modules, respectively.

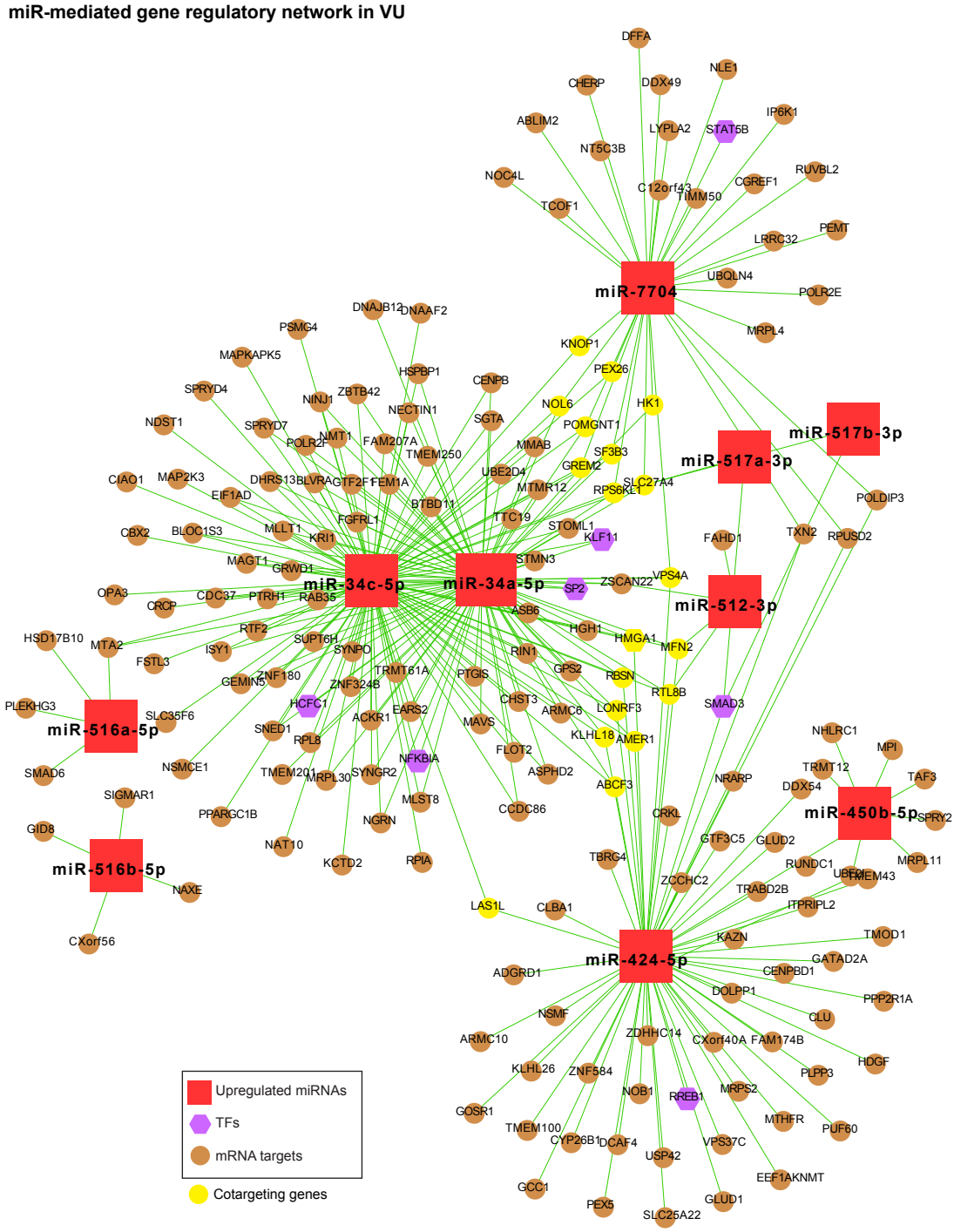

Fig. S6 MiR-mediated gene regulatory network in VU, which is constructed with the upregulated miRNAs in Fig. 4b, the mRNAs predicted as the strongest targets and with anti-correlated expression patterns (Pearson correlation, *P-value* < 0.05 and r < 0) with these miRNAs in human wounds, and the transcription factors (TFs) regulating these miRNAs' expression from the TransmiR v2 database (related to Fig. 4b–c and Additional file 8). The mRNAs co-targeted by miRNAs with unrelated seed sequences are highlighted in yellow.

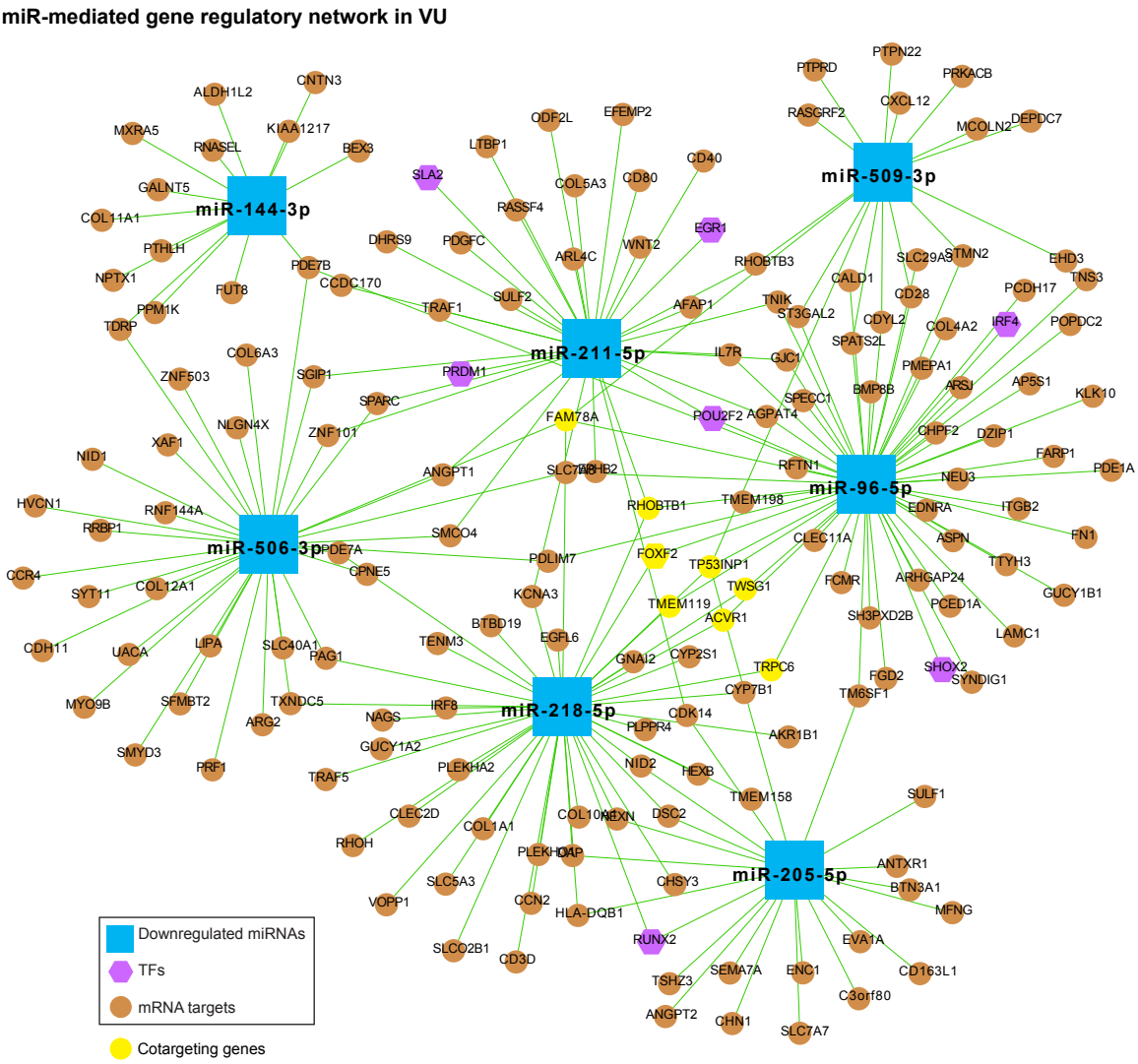

1043

1044 **Fig. S7 MiR-mediated gene regulatory network in VU**, which is constructed with the downregulated
1045 miRNAs in Fig. 4b, the mRNAs predicted as the strongest targets and with anti-correlated expression
1046 patterns (Pearson correlation, *P-value* < 0.05 and r < 0) with these miRNAs in human wounds, and the
1047 transcription factors (TFs) regulating these miRNAs' expression from the TransmiR v2 database
1048 (related to Fig. 4b–c and Additional file 8). The mRNAs co-targeted by miRNAs with unrelated seed
1049 sequences are highlighted in yellow.

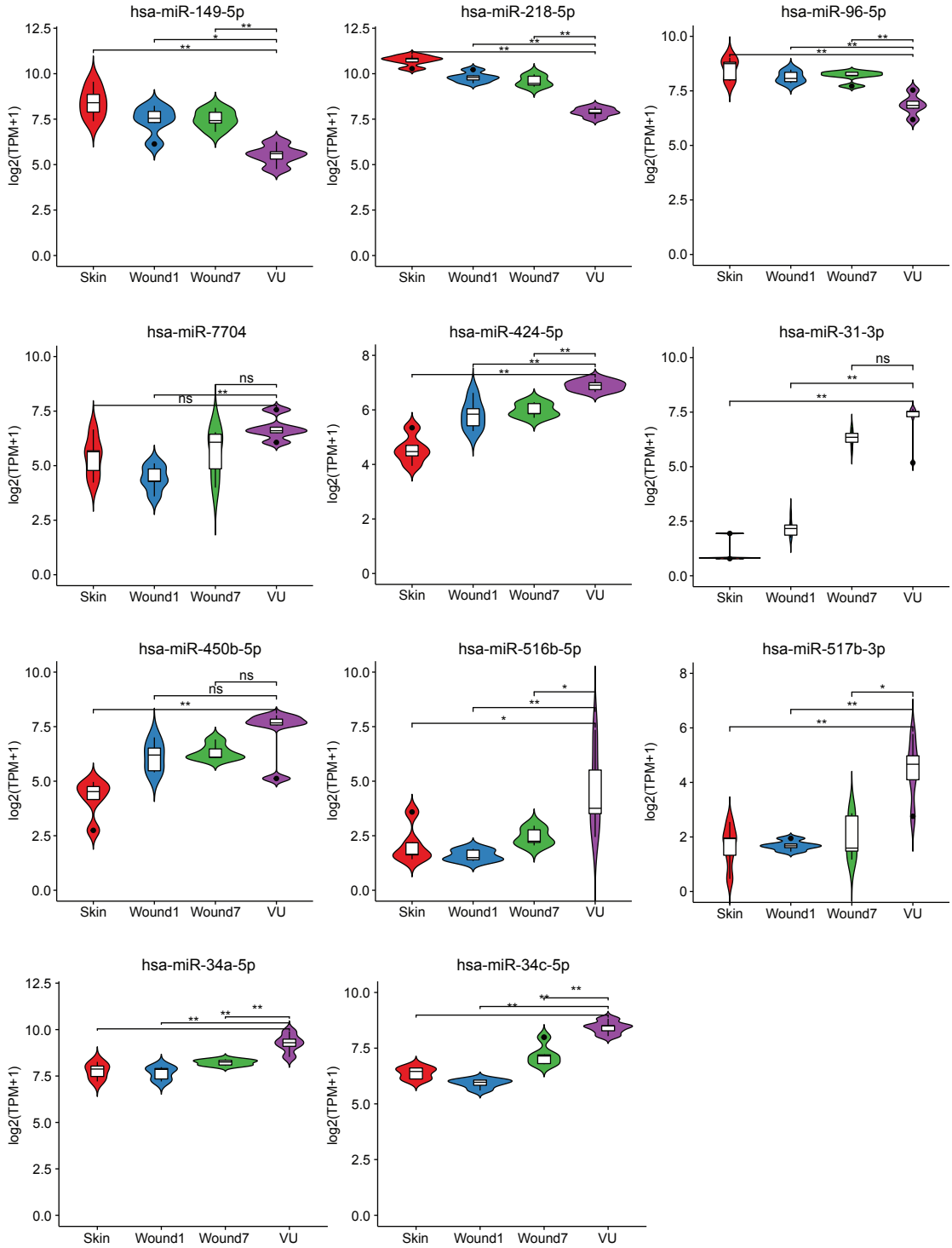

Fig. S8 RNA-sequencing results for the miRNAs selected for experimental validation (related to Fig. 5). Mann-Whitney t-test, *P < 0.05, **P < 0.01, ns: not significant.

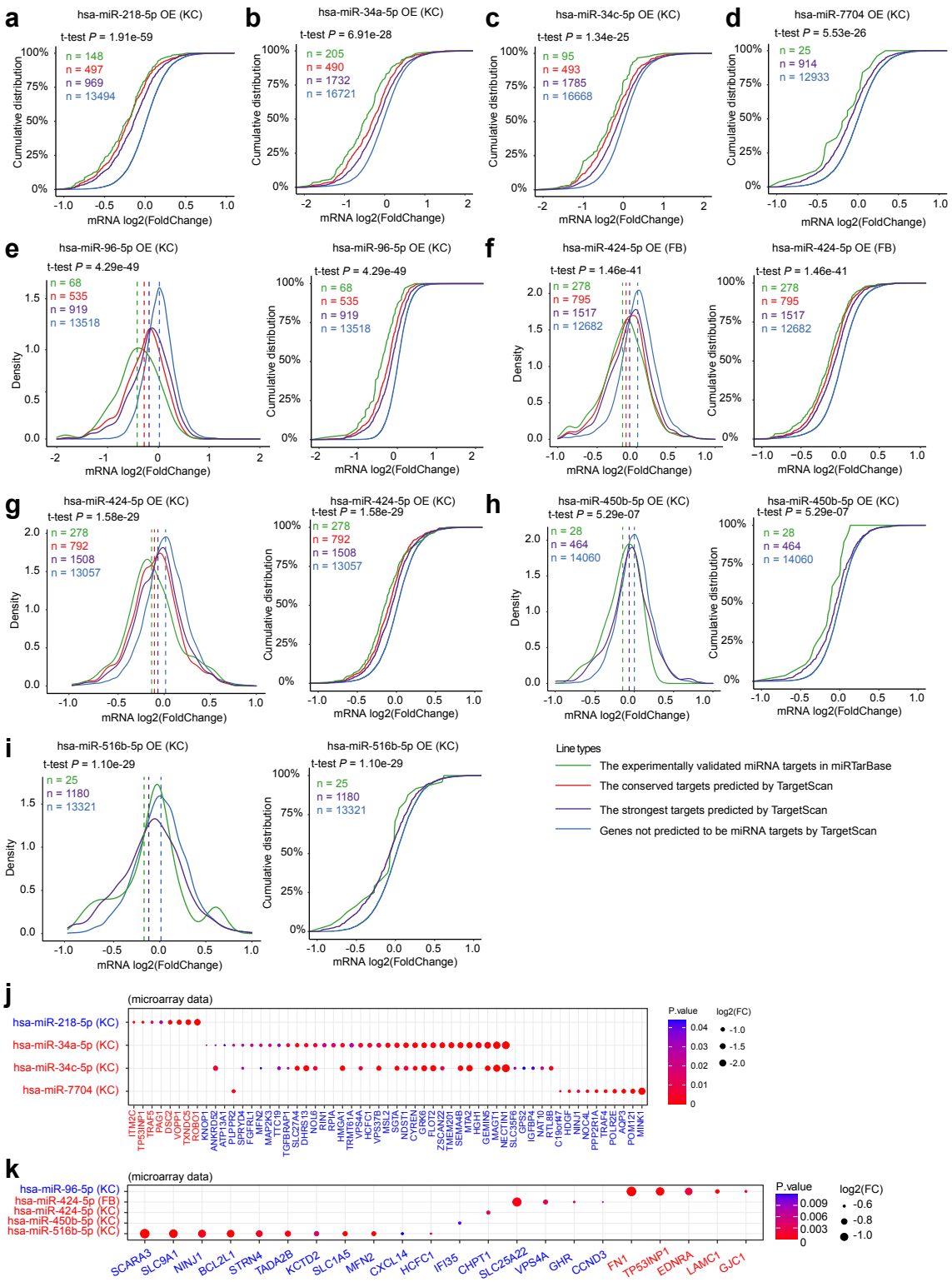

Fig. S9 Experimental validation of miRNAs' targetome (related to Fig. 5). Microarray analysis was performed in keratinocytes (KC) or fibroblasts (FB) with miR-218-5p (**a**), miR-34a-5p (**b**), miR-34c-5p (**c**), miR-7704 (**d**), miR-96-5p (**e**), miR-424-5p (**f, g**), miR-450-5p (**h**), or miR-516-5p (**i**) overexpression (OE). Density plots (left) and cumulative distributions (right in **e–i**) of mRNA log2(fold change) are shown.

1058 Wilcoxon t-tests were performed to compare the TargetScan predicted strongest targets (purple) with
1059 the non-targets (blue) for each of these miRNAs. The conserved and experimentally validated targets
1060 are marked with red and green colors, respectively. Dotted lines depict the average log2(fold change)
1061 values for each mRNA group. **j, k** The target mRNAs are significantly changed (fold change < -1.2 and
1062 *P*-value < 0.05) by the indicated miRNAs in the microarray analysis.

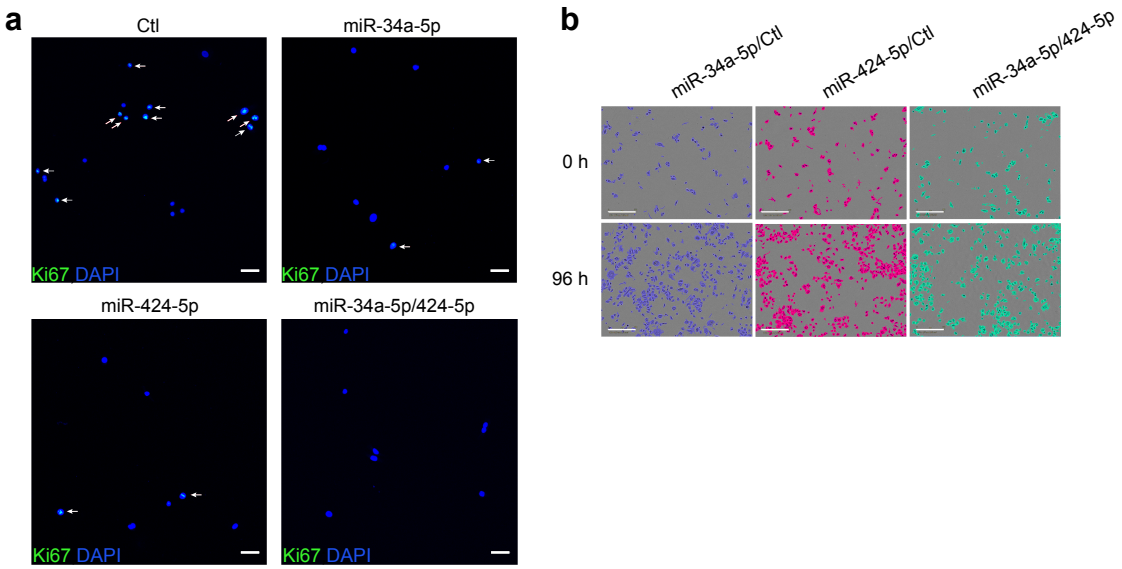

Fig. S10 Cooperation of miR-34a and miR-424 in regulating keratinocyte proliferation (related to Fig. 7). **a** Ki67 expression was detected in keratinocytes transfected with miR-34a-5p or miR-424-5p mimics alone or both mimics for 24 hours by immunofluorescence staining. Cell nuclei were costained with DAPI. Ki67+ cell nuclei are highlighted with white arrows in the representative photographs. (Scale bar: 50 μm.) **b** The growth of the transfected keratinocytes (n = 3) was analyzed with a live cell imaging system, and representative photographs of cells at 0 and 96 hours are shown (Scale bar, 300 μm.).

Table S1. **Characteristics of the healthy donors and the VU patients.**

Characteristics	Healthy donors	Patients with VU
Study population (n)	10	12
Age, years (mean ± s.d.)	65.3 ± 3.2	75.8 ± 12.0
Ethnicity	White	White
Gender (male: female)	2:8	5:7
Biopsy location	Lower leg	Lower leg
Wound duration	Acute (1 or 7 days after injury)	3.7 ± 5.3 years

Abbreviations: s.d., standard deviation; VU, venous ulcer.

1070

1071 **Table S2. Characteristics of the patients with venous ulcer.**

Patient	Sex	Age (years)	Ethnicity	Wound size (cm)	Wound duration (years)	Wound location	Experiment
1	M	86	Caucasian	6x5	4	Lower leg	RNA-seq & qRT-PCR
2	F	68	Caucasian	15x15	2	Lower leg	RNA-seq & qRT-PCR
3	M	70	Caucasian	3x0.5	0.3	Lower leg	RNA-seq & qRT-PCR
4	F	78	Caucasian	15x12	1.5	Lower leg	RNA-seq & qRT-PCR
5	F	87	Caucasian	3x2+8x4	2.5	Lower leg	RNA-seq & qRT-PCR
6	F	73	Caucasian	3x4	3.5	Lower leg	qRT-PCR
7	M	99	Caucasian	20x10	0.5	Lower leg	qRT-PCR
8	F	71	Caucasian	20x20	20	Lower leg	qRT-PCR
9	F	77	Caucasian	2.5x3+15x15	4.5	Lower leg	qRT-PCR
10	M	51	Caucasian	2x1.5	3	Lower leg	qRT-PCR
11	M	69	Caucasian	12x15	1	Lower leg	qRT-PCR
12	F	81	Caucasian	7x2.5	1	Lower leg	qRT-PCR

1072 Abbreviations: M, male; F, female.

1073 **Table S3. Characteristics of the healthy donors.**

Donor	Sex	Age (years)	Ethnicity	Wound location	Experiment
1	F	66	Caucasian	Lower leg	RNA-seq
2	M	69	Caucasian	Lower leg	RNA-seq
3	F	67	Caucasian	Lower leg	RNA-seq
4	M	69	Caucasian	Lower leg	RNA-seq & qRT-PCR
5	F	64	Caucasian	Lower leg	RNA-seq & qRT-PCR
6	F	60	Caucasian	Lower leg	qRT-PCR
7	F	66	Caucasian	Lower leg	qRT-PCR
8	F	60	Caucasian	Lower leg	qRT-PCR
9	F	67	Caucasian	Lower leg	qRT-PCR
10	F	65	Caucasian	Lower leg	qRT-PCR

1074 Abbreviations: M, male; F, female.

1075 **Table S4. Quality control of small RNA sequencing data.**

Groups	Sample name	Raw reads	Q20	Q30	GC content	Clean reads	Mapped reads	%Mapped rate
VU	VU1	12352608	96.83%	93.54%	53.05%	8592627	1478783	17.21
VU	VU2	10984280	96.87%	93.62%	52.11%	7924433	1842502	23.25
VU	VU3	13311104	96.85%	93.61%	51.73%	10756575	2284593	21.24
VU	VU4	11251717	96.60%	93.20%	53.50%	9426308	1847827	19.60
VU	VU5	16589164	96.88%	93.65%	51.80%	14041875	2710757	19.31
Skin	Skin1	17149375	95.05%	89.96%	51.70%	15180413	5807660	38.26
Skin	Skin2	11007535	95.55%	91.17%	50.69%	9876104	6993832	70.82
Skin	Skin3	10755030	95.82%	91.59%	51.60%	9246046	4878001	52.76
Skin	Skin4	10577666	96.92%	93.73%	52.87%	9125424	3288691	36.04
Skin	Skin5	14453350	97.00%	93.99%	51.00%	12409530	6733966	54.26
Wound1	Wound1_1	11631465	96.76%	93.38%	51.62%	9228914	4448460	48.20
Wound1	Wound1_2	10202264	97.00%	93.91%	50.08%	8894857	6258419	70.36
Wound1	Wound1_3	10173871	96.98%	93.77%	50.48%	8499570	5852107	68.85
Wound1	Wound1_4	11371432	96.90%	93.71%	50.77%	10256444	6620450	64.55
Wound1	Wound1_5	12469709	96.88%	93.68%	51.57%	10400310	4957568	47.67
Wound7	Wound7_1	11734696	96.89%	93.68%	51.13%	9884324	4099639	41.48
Wound7	Wound7_2	11312106	97.08%	94.07%	50.42%	9875669	5397518	54.66
Wound7	Wound7_3	11326902	96.89%	93.66%	51.28%	8587464	3942153	45.91
Wound7	Wound7_4	11073271	96.85%	93.54%	52.31%	8632616	2296446	26.60
Wound7	Wound7_5	12543302	96.85%	93.58%	51.70%	9564730	2811963	29.40

1076 Raw reads, clean reads, and mapped reads are single fragments.

1077 **Table S5. Quality control of rRNA-depleted total RNA sequencing data.**

Groups	Sample names	Total raw reads	Total clean reads	Clean data rate (%)	Input reads	Uniquely mapped reads	Uniquely mapped rate(%)
VU	VU1	101622474	95087574	0.94	47543787	41697735	0.877
VU	VU2	101685312	92173926	0.91	46086963	35158771	0.7629
VU	VU3	132592006	126190658	0.95	63095329	55771525	0.8839
VU	VU4	108786868	103438880	0.95	51719440	43012289	0.8316
VU	VU5	108416676	101355626	0.93	50677813	41194500	0.8129
Skin	Skin1	138065658	129299094	0.94	64649547	55300913	0.8554
Skin	Skin2	102996410	97056760	0.94	48528380	38950588	0.8026
Skin	Skin3	123478422	116018720	0.94	58009360	47207545	0.8138
Skin	Skin4	129515874	115240764	0.89	57620382	48834112	0.8475
Skin	Skin5	109239608	103341784	0.95	51670892	44434490	0.86
Wound1	Wound1_1	105127142	100922792	0.96	50461396	44012941	0.8722
Wound1	Wound1_2	104542368	100678896	0.96	50339448	44040712	0.8749
Wound1	Wound1_3	126002796	119469842	0.95	59734921	51566913	0.8633
Wound1	Wound1_4	103667154	98633466	0.95	49316733	41945529	0.8505
Wound1	Wound1_5	111446060	106610264	0.96	53305132	45076334	0.8456
Wound7	Wound7_1	115447748	109997276	0.95	54998638	45453970	0.8265
Wound7	Wound7_2	104662588	100033286	0.96	50016643	42515374	0.85
Wound7	Wound7_3	102504766	97652674	0.95	48826337	42134005	0.8629
Wound7	Wound7_4	108449990	103504388	0.95	51752194	43379024	0.8382
Wound7	Wound7_5	129466364	123563104	0.95	61781552	51511479	0.8338

1078 Raw reads, clean reads, input reads, and mapped reads are paired fragments.

1079 **Legend for Additional file 11**. **Keratinocyte growth was analyzed with a live cell**
1080 **imaging system.** 1, Keratinocytes co-transfected with miR-34a-5p and control mimics.
1081 2, Keratinocytes co-transfected with miR-424-5p and control mimics. 3, Keratinocytes
1082 co-transfected with miR-34a-5p and miR-424-5p mimics.